



**HAL**  
open science

## Sedimentological and palynological records since 10 ka BP along a proximal-distal gradient on the Armorican shelf (NW France)

Ophélie David, Aurélie Penaud, Muriel Vidal, Wiem Fersi, Clément Lambert, Evelyne Goubert, Maiwenn Herlédan, Pierre Stéphan, Yvan Pailler, Jean-François Bourillet, et al.

### ► To cite this version:

Ophélie David, Aurélie Penaud, Muriel Vidal, Wiem Fersi, Clément Lambert, et al.. Sedimentological and palynological records since 10 ka BP along a proximal-distal gradient on the Armorican shelf (NW France). *Quaternary Science Reviews*, 2022, 293, 10.1016/j.quascirev.2022.107678 . insu-03824739

**HAL Id: insu-03824739**

**<https://insu.hal.science/insu-03824739>**

Submitted on 21 Oct 2022

**HAL** is a multi-disciplinary open access archive for the deposit and dissemination of scientific research documents, whether they are published or not. The documents may come from teaching and research institutions in France or abroad, or from public or private research centers.

L'archive ouverte pluridisciplinaire **HAL**, est destinée au dépôt et à la diffusion de documents scientifiques de niveau recherche, publiés ou non, émanant des établissements d'enseignement et de recherche français ou étrangers, des laboratoires publics ou privés.

## Sedimentological and palynological records since 10 ka BP along a proximal-distal gradient on the Armorican shelf (NW France)

David Ophélie <sup>1,2,\*</sup>, Penaud Aurélie <sup>1</sup>, Vidal Muriel <sup>1</sup>, Fersi Wiem <sup>1</sup>, Lambert Clément <sup>2</sup>, Goubert Evelyne <sup>2</sup>, Herlédan Maiwenn <sup>3</sup>, Stéphan Pierre <sup>4</sup>, Pailler Yvan <sup>5</sup>, Bourillet Jean-François <sup>6</sup>, Baltzer Agnès <sup>7</sup>

<sup>1</sup> Geo-Ocean, Univ. Brest, CNRS, Ifremer, UMR 6538, F-29280 Plouzané, France

<sup>2</sup> Geo-Ocean, Univ. Bretagne Sud, Univ. Brest, CNRS, Ifremer, UMR 6538, F-56000 Vannes, France

<sup>3</sup> Univ. Lille, Laboratoire D'Océanologie et de Géosciences, UMR 8187, F-59655 Villeneuve d'Ascq, France

<sup>4</sup> CNRS, Littoral Environnement Télédétection Géomatique, UMR 6554, IUEM, F-29280 Plouzané, France

<sup>5</sup> Chaire Armerie, Univ. Brest, Inrap, Littoral Environnement Télédétection Géomatique, UMR 6554, IUEM, F-29280 Plouzané, France

<sup>6</sup> Ifremer, Ressources Physiques et écosystèmes de Fond de Mer, Centre de Bretagne. 1625, Route de Ste Anne, CS 10070, F-29280 Plouzané, France

<sup>7</sup> Univ. Nantes, Laboratoire Géolittomer/IGARUN, UMR 6554, F-44300 Nantes, France

\* Corresponding author : Ophélie David, email address : [ophelie.david@univ-ubs.fr](mailto:ophelie.david@univ-ubs.fr)

[aurelie.penaud@univ-brest.fr](mailto:aurelie.penaud@univ-brest.fr) ; [muriel.vidal@univ-brest.fr](mailto:muriel.vidal@univ-brest.fr) ; [wiem.fersi@univ-brest.fr](mailto:wiem.fersi@univ-brest.fr) ; [clement.lambert@univ-ubs.fr](mailto:clement.lambert@univ-ubs.fr) ; [evelyne.goubert@univ-ubs.fr](mailto:evelyne.goubert@univ-ubs.fr) ; [maiwenn.herledan.etu@univ-lille.fr](mailto:maiwenn.herledan.etu@univ-lille.fr) ; [pierre.stephan@univ-brest.fr](mailto:pierre.stephan@univ-brest.fr) ; [yvan.pailler@inrap.fr](mailto:yvan.pailler@inrap.fr) ; [jean.francois.bourillet@ifremer.fr](mailto:jean.francois.bourillet@ifremer.fr) ; [agnes.baltzer@univ-nantes.fr](mailto:agnes.baltzer@univ-nantes.fr)

### Abstract :

New findings acquired in Armorican shelf (core MD08-3204 CQ: Bay of Quiberon and core VK03-58bis: South Glénan islands) depict Holocene paleoenvironmental changes since 10 ka BP through a multi-proxy dataset including sedimentological and palynological data. First, grain-size analyses and AMS-14C dates show a common sedimentary history for both study cores. The slowdown of the relative sea level (RSL) rise was accompanied by a drop of the sedimentation rates between ~8.3 and 5.7 ka BP; the rates had been relatively higher at the onset of the Holocene. This interval led to the establishment of a shell-condensed level, identified in core VK03-58bis by the “Turritella layer” and interpreted as a marker for the Maximum Flooding Surface. Palynological data (pollen and dinoflagellate cyst assemblages) acquired in core MD08-3204 CQ argue for an amplification of the fluvial influence since 5.7 ka BP; the establishment of the Highstand System Tract (i.e., mixed marine and fluvial influences on the platform) then accompanied the slowdown of the RSL rise rates. On the shelf, the amplification of Anthropogenic Pollen Indicators (API) has been better detected since 4.2 ka BP, due not only to the increase of human impact but also due to a stronger fluvial influence on the shelf during the Late Holocene. Palynological data, recorded on the 8.5–8.3 ka BP interval along an inshore-offshore gradient, also demonstrate the

---

complexity of the palynological signals such as i) the fluvial influence that promotes some pollen taxa (*Alnus* and *Corylus*) from proximal areas and ii) the macro-regionalization of palynomorph sources in distal cores. In addition, the comparison of palynological tracers, including API, over the last 7 kyrs BP, with South Brittany coastal and mid-shelf sites subject to northern vs. southern Loire catchment areas, shows a major hydro-climatic effect on the reconstructed palynological signals. Strengthened subpolar gyre (SPG) dynamics, combined with recurrent positive North Atlantic Oscillation (NAO) configurations, appear responsible for increased winter precipitation and fluvial discharge over northern Europe, as in Brittany. Conversely, weakened SPG intervals, associated with recurrent negative NAO-like modes, are characterized by intensified winter fluvial discharge over southern Europe. Interestingly, at an infra-orbital timescale, we record major peaks of API during periods of strengthened (/weakened) SPG dynamics in sites subject to detritic-organic matter inputs from Brittany (/Loire) watersheds.

### Highlights

► The Armorican shelf sedimentation reflects the Holocene relative sea level rise. ► The condensed “*Turritella* layer” testifies of the Maximum Flooding Surface. ► Distortion of palynological signals from proximal to distal environments. ► The hydro-climatic forcing affects the anthropogenic pollen signal in shelf sediments. ► The Bronze and Middle Ages are recorded as main steps in human activity increase.

**Keywords** : Holocene, South Brittany, Pollen, Dinoflagellate cysts, Paleoenvironmental changes, *Turritella* layer, Anthropogenic pollen indicators (API), Fluvial discharge

## 61        **1. Introduction**

62        The Holocene (i.e., the last 11.7 kyrs BP) is characterized by climate variability operating  
63        differently according to timescales. In the first instance, the summer insolation at 65°N  
64        gradually decreases during the Holocene and induces a drop in Northern Hemisphere summer  
65        air temperatures (*Berger and Loutre, 1991*) fostering the Mid-Holocene freshening and the  
66        increase in winter precipitation over Northwestern (NW) Europe (e.g., *Morzadec-Kerfourn,*  
67        *1974; Naughton et al., 2007; Penaud et al., 2020*). Superimposed on the long-term Holocene  
68        climate trend, millennial-scale abrupt climate events derive from repeated cryospheric  
69        instabilities (i.e., Bond events, *Bond et al., 1997*; or Rapid Climate Changes with a more global-  
70        scale perspective, *Mayewski et al., 2004*). Over Europe, the infra-orbital Holocene climate  
71        subsequently oscillates at multidecadal timescales and is mainly driven by North Atlantic  
72        Oscillation-like (NAO; e.g., *Hurrell, 1995; Hurrell et al., 2003*) varying atmospheric regimes  
73        (e.g., *Olsen et al., 2012; Morley et al., 2014*) and North Atlantic Ocean gyre dynamics (e.g.,  
74        *Hátún et al., 2005; Thornalley et al., 2009; Moffa-Sánchez and Hall, 2017; Penaud et al., 2020;*  
75        *Lambert et al., 2020*).

76        Following the deglaciation, the Early Holocene is also characterized by high Relative Sea Level  
77        (RSL) rise rates that decreased during the Mid to Late Holocene along the Atlantic coasts (e.g.,  
78        Caribbean region and South America, *Milne et al., 2005*; Southern Bay of Biscay; *Leorri et al.,*  
79        *2012a, b*; North-America, *Engelhart et al., 2015*; Europe, *García-Artola et al., 2018*). The RSL  
80        evolution is strongly controlled by meltwater inputs and isostatic adjustments, inducing  
81        different sea-level rates according to the regions investigated (*Leorri et al., 2012a, b; Goslin et*  
82        *al., 2015; García-Artola, 2018*). Along the southern Brittany coasts (*García-Artola et al.,*  
83        *2018*), the RSL rose rapidly between 20 ka BP (~ -25 m) and ~7 ka BP (~ -5 m) and  
84        subsequently slowed down at ~6 ka BP (*Goslin et al., 2015; Stéphan et al., 2015; García-Artola*  
85        *et al., 2018*), leading to the development of tidal flats in estuarine environments and saltmarshes

86 along the European coasts (e.g., *Joly and Visset, 2009; Menier et al., 2010; Stéphan et al., 2019;*  
87 *Penaud et al., 2020*). The Holocene marine transgression thus progressively flooded fluvial  
88 paleovalleys, resulting in the geomorphological transformation of French Atlantic coastal  
89 ecosystems (e.g., *Proust et al., 2001; Weber et al., 2004; Chaumillon et al., 2008; Menier, 2004;*  
90 *Menier et al., 2010; Baltzer et al., 2014; Gregoire et al., 2017*).

91 Superimposed on these natural forcings, Holocene paleoenvironments are impacted by the  
92 evolution of human societies (i.e., cultural and technical changes), especially since the start of  
93 the Neolithic (i.e., ~7 ka BP in Brittany; *Pailler et al., 2008*). The related landscape changes  
94 are mainly recorded thanks to palynological data highlighting the progressive deforestation and  
95 the introduction and intensification of the agro-pastoral activities thanks to Anthropogenic  
96 Pollen Indicators (API) (e.g., *Marguerie, 1992; Visset et al., 1995, 1996; Gaudin, 2004; Visset*  
97 *and Bernard, 2006; Naughton et al., 2007; Fernane et al., 2014, 2015; Penaud et al., 2020*). In  
98 parallel with terrestrial bio-indicators (pollen grains), aquatic bio-indicators (dinoflagellate  
99 cysts or dinocysts) allow discussing surface water evolution through time linked with sea level  
100 variations or leaching of nutrients from soils to coastal waters (e.g., *Lambert et al., 2018;*  
101 *Penaud et al., 2020*). These latter paleoceanographic tracers are found in worldwide sediments  
102 and their distribution are mainly driven by sea-surface parameters (i.e., temperature, salinity),  
103 nutrient concentration and primary productivity regimes, as well as inshore-offshore gradients  
104 (e.g., *Zonneveld et al., 2013; Van Nieuwenhove et al., 2020; Marret et al., 2020; de Vernal et*  
105 *al., 2020*). Along the Brittany coasts, the modern distribution of dinocysts has recently been  
106 updated (*Ganne et al., 2016; Lambert et al. 2017, 2022*). Furthermore, *Penaud et al. (2020)*  
107 have recently classified dinocyst taxa into ecological groups according to different bathymetric  
108 contexts (i.e., estuarine, shallow bay, inner neritic, outer neritic, full oceanic) along a marine  
109 (distal or offshore) to coastal (proximal) temporal transect across the Bay of Biscay.

110 The Armorican shelf, subject to both fluvial (i.e., mainly the Loire and Vilaine rivers) and  
111 oceanic (i.e., North Atlantic Ocean through gyre dynamics) influences (Fig. 1a), is a key area  
112 for conducting paleoenvironmental studies (*Naughton et al., 2007; Penaud et al., 2020*). In this  
113 study, we examine two cores retrieved in the Armorican shelf (Figs. 1a, b): cores MD08-3204  
114 CQ (Bay of Quiberon) and VK03-58bis (Grande Vasière, South Glénan sector). Previous  
115 studies conducted on core VK03-58bis aimed at discussing the sedimentological structure of  
116 the Grande Vasière (*Folliot, 2004; Bourillet et al., 2005, 2006*) as well as landscape-climate  
117 changes in northwestern France (*Naughton et al., 2007*). Core MD08-3204 CQ was previously  
118 examined by *Baltzer et al. (2014)* to reconstruct the sedimentary filling of the Bay of Quiberon.  
119 The present work is based on i) new radiocarbon dates obtained for both studied cores and ii)  
120 new palynological (pollen and dinocyst) analyses conducted on core MD08-3204 CQ. Our first  
121 objective is to refine the chronostratigraphy of both sequences to reconstruct the sedimentary  
122 dynamics on the shelf in relation with the long-term evolution of the RSL rise. This allows  
123 providing a new stratigraphical significance for the “*Turritella* layer”, an interval characterized  
124 by a high concentration of *Turritella communis* shells in core VK03-58bis (*Folliot, 2004;*  
125 *Bourillet et al., 2005, 2006; Naughton et al., 2007; Baltzer et al., 2015*). Secondly, this study  
126 aims at understanding palynological signatures along a proximal-distal gradient from coastal  
127 (*Lambert et al., 2019; this study*), mid-shelf (*Naughton et al., 2007*) to deep marine  
128 environments (*Zumaque et al., 2017; Fersi et al., in prep*) on the 8.5–8.3 ka BP interval. Finally,  
129 the API detection is discussed from continental (South Brittany maritime marsh; *Fernane et al.,*  
130 *2015*) to Armorican shelf environments (*Penaud et al., 2020; this study*) over the last 7 kyrs BP  
131 taking into account anthropogenic and natural forcing.

132

## 133        **2. Environmental context**

### 134        **2.1. Hydrographical context of the Bay of Biscay**

135        The study area extends from the northern part of the Bay of Biscay (BoB), an open oceanic  
136        basin in the north-eastern Atlantic Ocean, to the coastal zone of South Brittany. In the BoB,  
137        modern residual shelf currents (Fig. 1a) depend on wind-driven, tidally-induced, and density-  
138        driven flows (*Pingree and Le Cann, 1989; Koutsikopoulos and Le Cann, 1996; Castaing et al.,*  
139        *1999*). Currently, seasonal atmospheric dynamics (*Pingree and Le Cann, 1989*) and river  
140        discharge (*Lazure and Jégou, 1998; Lazure et al., 2008*) lead to the complex hydrological  
141        system presented in *Charria et al. (2013)*. In winter (i.e., October to March), a SW-dominant  
142        wind regime forces a SE to NW shelf current as schematized in Fig. 1a, while in summer (i.e.,  
143        April to September), a NE-dominant wind regime forces a NW to SE shelf current (*Charria et*  
144        *al., 2013; Charria, 2018*). From mid-autumn to early spring, freshwater discharge of the Loire  
145        and Gironde rivers (i.e., values greater than 1500 m<sup>3</sup>/s; *Castaing and Allen, 1981*) are pushed  
146        back toward the BoB coastal areas under the influence of sustained wind activity (Fig. 1a). This  
147        leads to a salinity decrease and a sea-surface cooling between the coast and the 100 m isobath.  
148        Under increasing winter fluvial discharge, the establishment of the resulting modern “winter  
149        horizontal thermohaline front” then characterizes the pronounced disconnection of oceanic and  
150        shelf waters (*Castaing et al., 1999; Costoya et al., 2016; Fig. 1a*), identified from 3.3 ka BP on  
151        the mid-shelf (*Mojtahid et al., 2019; Penaud et al., 2020*).

152

### 153        **2.2. Sedimentological context of the Armorican shelf**

#### 154        **2.2.1. The Bay of Quiberon (BQ)**

155        The Bay of Quiberon (BQ; 4 to 14 km width) is located in the internal domain of the Armorican  
156        shelf, between the coast and the 50 m isobath (Figs. 1a, b). This shallow internal domain is

157 divided into two sectors separated by large paleovalley networks and weakly incised (*Guilcher,*  
158 *1948; Vanney, 1977; Menier, 2004; Menier et al., 2010, 2014*): i) the inshore region with water  
159 depths below 25 m (i.e., bays of Quiberon and Vilaine; Fig. 1b) and ii) the offshore region  
160 formed by rocky shoals (i.e., islands of Houat and Hoëdic; Fig. 1b). In the BQ, modern  
161 sedimentation consists of fine terrigenous sediments (i.e., muddy sand; Fig. 1b), coming mainly  
162 from the swells-driven resuspension of the fine sediments deposited in the Vilaine Bay and  
163 from the Morbihan Gulf, Vilaine and Loire river plumes (*Menier et al., 2010, 2014*).

164 The Holocene sedimentary infilling of the BQ, following the Last Glacial Maximum (~20 ka  
165 BP) when the BQ was completely submerged, has been thoroughly studied using seismic  
166 profiles and sedimentological analyses (*Baltzer et al., 2014*). The BQ post-glacial flooding was  
167 initially confined to paleovalleys, gradually filled by fluvial deposits, which evolved to a  
168 subtidal bay (Unit 2 in *Baltzer et al., 2014*). Next, marine deposits indicative of energetic  
169 conditions (e.g., sparse marine shell debris, clayey- and sandy-rich deposits) settled during the  
170 rapid sea-level rise (8.7 to 6–5 ka BP; Unit 3 in *Baltzer et al., 2014*) until reaching the Maximum  
171 Flooding Surface (MFS). Following the RSL rise, BQ sedimentation now reflects highstand sea  
172 level conditions established since ~6–5 ka BP (Unit 4 in *Baltzer et al., 2014*).

173

### 174 **2.2.2. The Grande Vasière mid-shelf belt (GV)**

175 The Grande Vasière (GV; 225 km length; 40 km wide; surface of 8,000 km<sup>2</sup>; Fig. 1a), located  
176 between 80 and 110 m water depth, is a mid-depth mud belt (*McCave, 1972; Dubrulle et al.,*  
177 *2007*). The GV generally designates the upper part of the Holocene sediment accumulation built  
178 up at a rate of 0.1 to 0.2 cm/yr (*Lesueur et al., 2001*). The GV consists of a thin layer of silty  
179 mud, mainly tens of centimeters thick except on the NNW and SSE edges, overlying two sandy  
180 units (*Andreieff et al., 1971; Bourillet et al., 2006*). Present-day sediment inputs come from the



181 winter fluvial terrigenous supply ( $1.5 \cdot 10^6$  t/yr from the Gironde,  $0.5 \cdot 10^6$  t/yr from the Loire, and  
182  $0.1 \cdot 10^6$  t/yr from the Vilaine; *Jouanneau et al., 1999*) and the wave erosion (storminess and  
183 distant swell) of the NW French coast between April and September (*Jouanneau et al., 1999*;  
184 *Dubrulle et al., 2007*). In the BoB, the winter horizontal thermohaline front derives from the  
185 extension of winter fluvial turbid plumes up to the 100 m isobath (*Costoya et al., 2016*),  
186 explaining the extension of the mid-shelf sediment deposits on the GV (*Castaing et al., 1999*).  
187 The provisional sedimentary budget over the last 30 years shows a decrease of the clayey  
188 fraction due to the fine material remobilization because of storms and fishing activities  
189 (*Bourillet et al., 2006*).

190 In the northern part of the BoB, the Loire and Vilaine rivers together represent 95% of BoB  
191 watersheds. Up to 90% of the nutrient contribution in the northern part of the Armorican shelf  
192 comes from the Loire and Vilaine rivers and the southern Brittany coastal river discharge make  
193 smaller secondary contributions (*Guillaud et al., 2008*). The northernmost sector of the GV  
194 (southwest of Glénan islands; Fig. 1b) is characterized by a thicker, muddy layer, of a few  
195 meters of Holocene silty-clayey sediments (*Bourillet et al., 2006*). In this area, a characteristic  
196 acoustic reflector in seismic profiles has been identified and attributed to the presence of a  
197 remarkable concentration of *Turritella communis* shells, described as the “*Turritella* layer” in  
198 the core VK03-58bis (*Folliot, 2004*; *Bourillet et al., 2005, 2006*). The environmental changes  
199 required for the establishment of this shell deposit, observed on the Armorican shelf but also  
200 elsewhere in the northern Atlantic Ocean (Scottish fjords; *Baltzer et al., 2015*), are still debated.

201

## 202        **3. Material and methods**

### 203        **3.1. Studied cores**

204        The CALYPSO square (CASQ) core MD08-3204 CQ (47°30'27.6''N; 3°1'18.6''O; 17 m deep;  
205        8.91 m long) was collected in the central part of the BQ (Figs. 1a, b) onboard the R/V Marion  
206        Dufresne in 2008 (MD169/MICROSYSTEMS cruise; *Blamart et al., 2008*). Only the three  
207        upper meters are examined in this study.

208        The VK03-58bis core (47°36.349'N; 4°08.173'W; 96.8 m deep; 2.72 m long) was collected  
209        with a vibrocorer, in the NNW edge of the GV off the South Glénan islands (GV; Figs. 1a, b)  
210        during the Vibarmor cruise, onboard the R/V *Côtes de la Manche* (*Le Roy, 2003*; 'Défi Golfe  
211        de Gascogne' 2001-2005, Ifremer). The latter sedimentary archive retrieves the totality of the  
212        northern GV sediment accumulation (*Bourillet et al., 2005, 2006*; *Naughton et al., 2007*).

213

### 214        **3.2. Chronological frameworks**

215        New chronostratigraphies established on both studied cores were used to discuss the  
216        sedimentation dynamics on the Armorican shelf. In this study, 11 new AMS-<sup>14</sup>C dates were  
217        obtained for the upper three meters of core MD08-3204 CQ, these were used to build a robust  
218        chronostratigraphy based on a total of 15 AMS-<sup>14</sup>C dates between 287 and 20 cm (Table 1).  
219        Regarding core VK03-58bis, 10 additional AMS-<sup>14</sup>C dates were newly acquired (8 on benthic  
220        foraminifera and 2 on *Turritella communis* shells), complementing the 5 earlier AMS-<sup>14</sup>C dates  
221        published in *Naughton et al. (2007)* (Table 2). All AMS-<sup>14</sup>C dates were calibrated with the  
222        CALIB 7.1 software using the IntCal20 calibration curve (*Stuiver and Reimer, 1993*; *Reimer et*  
223        *al., 2020*), first considering a reservoir age of  $-400 \pm 45$  years to radiocarbon dates (point 1559  
224        for the lower Loire in the marine20 database; *Tisnérat-Laborde et al., 2010*) for both studied  
225        cores (Tables 1 and 2).

226 Also, this study aims at understanding palynological signatures along a proximal-distal gradient  
227 on the Armorican shelf since the subsequent RSL slowdown at ~6 ka BP. For this purpose, an  
228 age model was established on the top core section (134–20 cm) of core MD08-3204 CQ using  
229 the rbacon package (*Blaauw and Christen, 2011*) in R version 4.1.2 (R Development Core  
230 Team, 2021; <http://www.r-project.org/>). This allowed reconstructing the last 5.7 kyrs BP (Fig.  
231 2a), while no age model was established for the lower section of the core (287–134 cm) because  
232 of the peculiar sedimentological context discussed later in the manuscript (i.e., period of  
233 remobilization or no sediment deposition). The palynological records obtained on core MD08-  
234 3204 CQ were also compared with published palynological datasets from continental (core  
235 GL3, Loc'h of Guidel; *Fernane et al., 2015*) and mid-shelf (core CBT-CS11, Grande Vasière,  
236 Penmarc'h sector; *Penaud et al., 2020*) sedimentary archives (Figs. 1a, b). For the last two cited  
237 cores, all AMS-14C dates previously acquired were re-calibrated and their age models were  
238 modified using the same chronological methodologies as the one described for core MD08-  
239 3204 CQ (Fig. 2b).

240

### 241 **3.3. Sedimentological analyses**

242 In this study, the logs previously established for cores MD08-3204 CQ (*Baltzer et al., 2014*)  
243 and VK03-58bis (*Folliot, 2004*) were reviewed thanks to a refined description of the  
244 sedimentary facies (Figs. 3 a, b).

245 Regarding core MD08-3204 CQ, the sedimentological data presented in this study refer to the  
246 299–1 cm section also investigated for palynological data. Sedimentological analyses  
247 previously carried out on this core (*Baltzer et al., 2014*) include a sedimentological description  
248 and total grain-size analyses (after removal of the organic matter) using a Beckman-Coulter  
249 LS230 laser particle analyzer. Also, new calcimetry (% CaCO<sub>3</sub>; Fig. 3a) and Total Organic  
250 Carbon (% TOC; Fig. 3a) data were acquired (UMR 6249 Chrono-environnement laboratory,

251 Univ. Bourgogne Franche-Comté) thanks to the standard Loss On Ignition (LOI) method (*Heiri*  
252 *et al., 2001*). Sediments were dried at 105°C during 20 hours and then cooled in a dessicator  
253 before burning. After weighing, samples were burned at 550°C during 5 hours and weighed to  
254 calculate the TOC content. Then, the samples were burned at 950°C during 2 hours and weighed  
255 to calculate the carbonate content.

256 Regarding the VK03-58bis core, new CaCO<sub>3</sub>-free grain-size analyses (after HCl 30%  
257 treatment) were performed on a Malvern Hydro 2000 particle size analyzer (Univ. Bretagne  
258 Sud, Pontivy), and added information on previous sedimentological data including grain-size  
259 analyses on the total sediment fraction (*Bourillet et al., 2005; Naughton et al., 2007; Fig. 3b*).  
260 Grain-size statistics for both study cores, including median grain-size (D50) values, were  
261 obtained using the GRADISTAT v 8.0 software (*Blott and Pye, 2001*).

262

### 263 **3.4. Palynological analyses**

264 New palynological data were acquired on core MD08-3204 CQ (BQ; Fig. 1b) for the upper  
265 three meters of the core. A total of 61 samples were taken every 10–20 cm, in the lower part of  
266 the sequence (i.e., 290–140 cm), and every ~3 cm in the upper part (i.e., 140–10 cm) within a  
267 1 cm sample (i.e., corresponding to ~2 cm<sup>3</sup>).

268 Palynological treatments on the <150 µm sediment fraction were carried out at the Geo-Ocean  
269 laboratory (Univ. Bretagne Occidentale, Plouzané) following the procedure described by *de*  
270 *Vernal et al. (1999)*. First, carbonate and siliceous fractions were removed using chemical  
271 treatments (cold 10-25-50% HCl and cold 40-70% HF). Then, mineral clayey fractions were  
272 sieved with 10 µm mesh size nylon screens. An optical microscope Leica DMC 2500 at ×630  
273 magnification was used for palynomorph determination, following *Beug (1961)* and *Reille*  
274 *(1995)* for pollen and *Rochon et al. (1999)* and *Van Nieuwenhove et al. (2020)* for dinocyst

275 identifications. For each sample a minimum of i) 300 pollen grains (150 grains excluding *Pinus*  
276 and indeterminate grains; *Fatela and Taborda, 2002*) and ii) 300 dinocysts (100 specimens  
277 besides the dominant species *Lingulodinium machaerophorum*), were counted to systematically  
278 ensure statistically reliable assemblages (*Mertens et al., 2009*). Palynological results were then  
279 represented in absolute (number of specimens/cm<sup>3</sup>) and relative (percentages) abundances  
280 (Table 3). Palynological diagrams and cluster analyses were performed using the Psimpoll  
281 program (*Bennet, 1992*), and ecological indexes (number of taxa per sample, Margalef  
282 diversity, and dominance; Table 3) were calculated using the Past program v 1.75b (*Hammer*  
283 *et al., 2001*). The dinocyst and pollen identified in core MD08-3204 CQ are grouping according  
284 to their ecological affinities (see Table 3).

285

## 286 **4. Results**

### 287 **4.1. Sediment facies description and chrono-stratigraphical model**

#### 288 ***4.1.1. The MD08-3204 CQ core: the inshore domain of the Bay of Quiberon***

289 The age-depth plot (Fig. 3a) defines three main stratigraphical intervals. In the lower part,  
290 between 299–196 cm, a short time interval encompassing 200 years (8.5–8.3 ka BP) is  
291 characterized by high sedimentation rates of about 4.5 mm/yr. Between 196–134 cm (8.3–5.7  
292 ka BP), a drop in sedimentation rates (decreasing to ~0.2 mm/yr), associated with a reversed  
293 date, suggests a period of remobilization or no sediment deposition (grey band in Fig. 3a). From  
294 134 cm (5.7 ka BP) to the top of the core, a resumption of lower and constant sedimentation  
295 rates of about 0.24 mm/yr is calculated.

296 Regarding grain-size analyses performed on the total sediment fraction, in the lower part of the  
297 core between 299–250 cm, sediments consist of fine to medium sands, with less than 40% of  
298 silty-clayey sediments (Fig. 3a). Between 250–200 cm, a larger proportion of silty-clayey  
299 sediments (~60% of the grain size distribution) is characterized by an increase of the TOC  
300 (higher than 6%; Fig. 3a). Between 200–180 cm, marking the base of the low sedimentation  
301 rate interval, total sediment D50 values rise (~40  $\mu\text{m}$  before limit 1 and 150  $\mu\text{m}$  after this limit;  
302 Fig. 3a) and correspond to the increase of the proportion of fine to sands. From 180 cm,  
303 sediments consist in very fine-sandy (~60% of the grain size distribution, limit 2 in Fig. 3a).  
304 Finally, at 134 cm (i.e., limit 3 corresponds to the resumption of constant sedimentation rates),  
305 total sediment D50 values decrease (~95  $\mu\text{m}$  before limit 3 and 42  $\mu\text{m}$  after; Fig. 3a). At the  
306 same time, both calcimetry (4% before 134 cm and 12% after limit 3) and TOC (lower than 6%  
307 before 134 cm and between 6-12% after limit 3) increase.

308

309 **4.1.2. The VK03-58bis core in the mid-shelf mud belt (northern Grande Vasière)**

310 The age-depth plot of core VK03-58bis (Fig. 3b) defines three main stratigraphical intervals,  
311 as for core MD08-3204 CQ. The lower part, between 266–165 cm (10–8.4 ka BP), is  
312 characterized by higher sedimentation rates of about 0.6 mm/yr. Between 165–140 cm (8.4–6.3  
313 ka BP), an abrupt drop in sedimentation rates is observed (decreasing to 0.01 mm/yr; grey band  
314 in Fig. 3b). From 137 cm (6.3 ka BP) to the top of the core, a resumption of lower sedimentation  
315 rates of about 0.22 mm/yr is reconstructed, with values close to the ones calculated for the post-  
316 5.7 ka BP interval described for core MD08-3204 CQ (Fig. 3a).

317 Regarding grain-size analyses performed on the total sediment fraction, during the interval  
318 characterized by higher sedimentation rates (~0.6 mm/yr; Fig. 3b), sediments consist mainly of  
319 coarser silty sediments with clast debris whose sizes gradually decrease between 270–210 cm.  
320 Between ~210–170 cm (Fig. 3b), finer sediments are characterized by decreases of both CaCO<sub>3</sub>-  
321 free and total sediment D50 values. In addition, the interval characterized by a drop in  
322 sedimentation rates (~0.01 mm/yr; grey band in Fig. 3b), encompassing a remarkable 161–149  
323 cm level of *Turritella communis*, is marked by a rise of CaCO<sub>3</sub>-free and total sediment D50  
324 values (~18 µm before limit 1', and 30 µm after this limit). From the first appearance of *T.*  
325 *communis* at 213 cm, their shell concentration gradually increases until reaching the high  
326 concentrated level, known as the “*Turritella* layer” (TL; Bourillet *et al.*, 2005; Naughton *et al.*,  
327 2007; Baltzer *et al.*, 2015), visible on the X-Ray radiography (Bourillet *et al.*, 2005; Fig. 3b).  
328 A few *Turritella* shells, highly scattered, still occur above the TL horizon. From 140 cm  
329 onward, corresponding to the resumption of constant sedimentation rates of about 0.22 mm/yr  
330 (limit 2'; Fig. 3b), finer silty-clayey sediments are characterized by the decrease of total  
331 sediment D50 values (~30 µm before 140 cm and 18 µm after this limit).

332

## 333        **4.2. Palynological results of core MD08-3204 CQ**

334 The description of palynological results led to the examination of four main palynozones (MD1  
335 to MD4; Figs. 4 and 5). These zones were established based on pollen and dinocyst observations  
336 in terms of both concentrations (Fig. 4) and percentages (Fig. 5), coupled with a clustering  
337 analysis. The palynological data are not described and interpreted in the 196–134 cm interval  
338 (grey bands in Figs. 4 and 5) owing to potential taphonomic bias and possible remobilization  
339 (subsection 4.1.1.). The palynological data acquired in the 299–210 cm interval are not  
340 discussed from a stratigraphic point of view because of extremely high sedimentation rates.  
341 Moreover, this interval is marked by extremely low dinocyst concentrations (less than 50  
342 dinocysts counted per level in the 299–210 interval; Figs. 4a, f). For these reasons, the  
343 palynological data have been summed to get an average picture of the interval in the discussion  
344 hereafter. Owing to the constant sedimentation rates, the palynological (pollen and dinocysts)  
345 signal is analyzed at a 100-year time resolution from 140 cm onward.

346

### 347        **4.2.1. Diversity and concentrations**

348 A total of 31 different dinocyst taxa were recognized in the whole core, with a mean taxon  
349 richness of 14 dinocyst taxa per slide, with lower diversity before 134 cm (i.e., 5.7 ka BP) and  
350 higher diversity after this limit (Fig. 4c; and related higher Margalef diversity in Fig. 4b). Total  
351 dinocyst concentrations (Fig. 4a) range between ~300 and 53,000 cysts/cm<sup>3</sup>, with very low  
352 values estimated in the 290–196 cm interval (mean of 1,400 cysts/cm<sup>3</sup>; MD1 excluding the  
353 196–134 cm section). Higher concentrations are recorded in the upper part of the core, divided  
354 into three palynozones according to the main fluctuations of concentration values: MD2 (134–  
355 112 cm; 5.7–4.9 ka BP; mean of 4,600 cysts/cm<sup>3</sup>), MD3 (112–49 cm; 4.9–2.4 ka BP; mean of  
356 26,100 cysts/cm<sup>3</sup>) and MD4 (from 49 cm or 2.4 ka BP; mean of 9,200 cysts/cm<sup>3</sup>; Fig. 4a). Total



357 dinocyst concentrations (Fig. 4a; as well as the dominance index in Fig. 4d) are mainly  
358 influenced by *Lingulodinium machaerophorum* occurrences (Figs. 4a, e). Maximal dinocyst  
359 concentrations are therefore reached in zone MD3 (mean of 26,000 cysts/cm<sup>3</sup>), in parallel with  
360 maximal percentages of *L. machaerophorum* at ~96% (Fig. 4e). Due to the low dinocyst counts  
361 (far below 100 specimens/slide) reached in zone MD1 (Fig. 4f: mean of 28 dinocyst counts per  
362 slide for the 7 samples between 290–196 cm), the dinocyst data obtained across this 200 yr-  
363 long interval (8.5–8.3 ka BP) were summed (194 dinocysts) providing mean dinocyst  
364 percentages for this interval (Fig. 5a and the following description of results).

365 Regarding pollen analyses, 95 different taxa were recognized in total with an average of 25  
366 pollen taxa per slide, with lower diversity before limit a (134 cm) and higher diversity after this  
367 boundary (Fig. 4i; and related higher Margalef diversity in Fig. 4h). The maximal pollen  
368 diversity is recorded in zone MD4 (~26 different taxa per slide; Figs. 4h, i). Total pollen  
369 concentrations (Fig. 4g) range between ~2,700 and 38,000 grains/cm<sup>3</sup>, with high values  
370 reconstructed in zone MD1 (mean of 20,299 grains/cm<sup>3</sup>), and especially during the interval of  
371 finer sediments (mean of 29,500 grains/cm<sup>3</sup>) that are favorable to a higher concentration of  
372 palynomorphs. Considering the upper part of the core, after 134 cm (i.e., 5.7 ka BP), higher  
373 pollen concentrations are recorded in zone MD3 (112–49 cm; 4.9–2.4 ka BP; mean of 11,900  
374 grains/cm<sup>3</sup>), while MD2 (132–112 cm; 5.7–4.9 ka BP; mean of 8,000 grains/cm<sup>3</sup>) and MD4  
375 (from 49 cm or 2.4 ka BP; mean of 5,700 grains/cm<sup>3</sup>; Fig. 4g) are characterized by lower values.  
376 The pollen dominance index (Fig. 4j) is mainly determined by *Quercus* percentages (Fig. 4k)  
377 all along the core; the lowest values of this taxon being recorded in zone MD4, which is also  
378 characterized by the highest pollen diversity.

379

#### 380 4.2.2. Description of palynological assemblages

381 Zone MD1 is characterized by the dominance of inner neritic (~62%; i.e., *Spiniferites lazus*,  
382 *Spiniferites bentorii*) and outer neritic (~24%; i.e., *Operculodinium centrocarpum* sensu *Wall*  
383 *& Dale, 1966*, *Spiniferites mirabilis*) taxa (Fig. 5a). Above 134 cm, zone MD2 corresponds to  
384 increasing percentages of *L. machaerophorum* (mean of 77%) and the decrease of other  
385 dinocyst taxa (Fig. 5a). In zone MD3, *L. machaerophorum* reaches maximum values above  
386 80%, with two subzones that can be identified. In subzone MD3a, *L. machaerophorum* reaches  
387 its highest values in the whole study sequence (up to 95%), whereas subzone MD3b (80–49  
388 cm) is characterized by the progressive rise of inner neritic taxa, mainly due to increasing  
389 percentages of *S. bentorii* and *S. lazus*. Finally, zone MD4 (49 cm onward; from 2.4 ka BP) is  
390 marked by a decrease of *L. machaerophorum* percentages (mean of 74%), as well as an increase  
391 of *Spiniferites* taxa and coastal heterotrophic percentages (Fig. 5a), especially in subzone MD4b  
392 (i.e., from 30 cm).

393 Regarding pollen assemblages (Fig. 5b), zone MD1 is characterized by occurrences of  
394 Amaranthaceae (mean of 12%), and high percentages of arboreal taxa (average of 77%), mainly  
395 represented by *Quercus* and *Corylus*. Zone MD2 is marked by lower percentages of  
396 Amaranthaceae and increasing values of riparian tree taxa, mainly due to the gradual rise of  
397 *Alnus* (Fig. 5b). Zone MD3 is characterized by the highest values of riparian taxa (21%), while  
398 thermophilic trees *Ulmus* and *Tilia* progressively decline. In subzone MD3b, the decrease in  
399 arboreal taxa (i.e., *Quercus* and *Corylus*) and the increase in Poaceae percentages are  
400 particularly obvious. In addition, occurrences of *Fagus* are noted. In zone MD3b, the decline  
401 of the forest system is associated with the increase of ruderal and adventitious taxa and is  
402 amplified in zone MD4 (Fig. 5b). The latter zone is characterized by the rise of Poaceae and a  
403 sharp decrease in arboreal taxa percentages. Sub-palynozone MD4b stands out by the highest  
404 occurrences of cultivated taxa (4%).

## 405 **5. Discussion**

### 406 **5.1. Sedimentary evolution of the Armorican shelf over the last 10 kyrs BP**

#### 407 ***5.1.1. Sedimentation rates during the Holocene transgression***

408 In the high sedimentation rate interval (~10–8.4 ka BP), higher sedimentation rates are recorded  
409 in the BQ (~4.5 mm/yr; Fig. 3a) compared to the northern GV (~0.66 mm/yr; Fig. 3b). This can  
410 be explained by the proximity to the coast of core MD08-3204 CQ (~7 km from present day  
411 coastline) and the shallowest depositional environment (~17 m deep today), whereas core  
412 VK03-58bis lies farther (~22 km from present day coastline) and deeper (~96 m deep today).  
413 Moreover, fine to medium sand sediments are found in core MD08-3204 CQ, reflecting more  
414 energetic marine conditions during the flooding of the BQ, whereas at that time the GV was  
415 already located in an open oceanic area.

416 Similar trends in sedimentation rates, occurring in the same temporal windows in both study  
417 cores, reflect a shared sedimentary evolution related to the evolution of the RSL rise through  
418 time (see Fig. 3 with the southern Brittany RSL rise from *García-Artola et al., 2018*).  
419 Specifically, both age-depth plots (Fig. 3) evidence a period of high sedimentation rates i) in  
420 the 8.5–8.3 ka BP interval for core MD08-3204 CQ (~4.5 mm/yr) and ii) in the 10–8.3 ka BP  
421 interval for core VK03-58bis (~0.6 mm/yr). The fast rhythm of the transgression (~10 mm/yr)  
422 during the final step of the rapid RSL rise (*García-Artola et al., 2018*) led to high sedimentation  
423 rates associated with the establishment of the Transgressive System Tract (TST; Figs. 3 and 6).  
424 At that time, the occurrences of inner and outer neritic dinocyst taxa together with  
425 Amaranthaceae pollen (Figs. 5 and 6) testify that the BQ is a subtidal bay close to extended  
426 maritime marshes and detrital sources also explaining extremely high continental palynomorph  
427 fluxes to the BQ (Fig. 6). The TST establishment is also recorded in the Loire estuarine system

428 (*Delaine et al., 2015; Arthuis et al., 2015; Arthuis, 2020*) that extended in the Gulf of Morbihan  
429 from ~9 to 5.8–5 ka BP (*Perez-Belmonte, 2008*).

430 Subsequently, and until 5.7 ka BP, a drop in sedimentation rates is recorded in both studied  
431 cores (0.24 and 0.01 mm/yr for cores MD08-3204 CQ and VK03-58bis, respectively; Fig. 3)  
432 synchronously with the slowdown of the RSL rise rates, as regionally recorded at ~6 ka BP  
433 (*Goslin et al., 2015; Stéphan et al., 2015; García-Artola et al., 2018*). The Maximum Flooding  
434 Surface (MFS) marks the end of the general transgression, inducing a reduction of the  
435 accommodation space and leading to lower sediment deposition. For the MD08-3204 CQ core,  
436 the interval of slowing RSL rise and decreasing sedimentation rates is associated with a reversed  
437 date suggesting a period of remobilization. Thus, we suggest a revision for the BQ model  
438 established by *Baltzer et al. (2014)* that previously discussed the establishment of the MFS at  
439 ~5 ka BP (Fig. 3a). According to our new chronostratigraphy and the consistent signal obtained  
440 with the GV, the transgressive deposit (i.e. TST) ends at 8.3 ka BP, and is followed by a period  
441 of sediment remobilization (i.e., MSF establishment) until 5.7 ka BP.

442 Then, from 5.7 ka BP, a resumption of sedimentation, at lower rates (~0.24 mm/yr and 0.22  
443 mm/yr for cores MD08-3204 CQ and VK03-58bis, respectively) than during the pre-8.3 ka BP  
444 interval, occurs in a period of slower RSL rise (i.e., less than 1 mm/yr after 6 ka BP; *García-*  
445 *Artola et al., 2018*; Fig. 3) corresponding to the establishment of the Highstand System Tract  
446 (HST; Figs. 3 and 6). The increase of the continental-fluvial influence is observed over the  
447 Armorican shelf through higher percentages (Figs. 5a and 6) and fluxes (Fig. 6) of *L.*  
448 *machaerophorum*, almost monospecific today in estuarine sediments (*Morzadec-Kerfourn,*  
449 *1976, 1977; Ganne et al., 2016; Lambert et al., 2017*), and of riparian pollen taxa (Fig. 5b), as  
450 recently discussed on the Armorican mid-shelf (*Penaud et al., 2020*). At the same time, high  
451 erosional episodes identified in the Gulf of Morbihan, and the Loire estuary, testify to a

452 predominant runoff and fluvial discharge to the Bay of Biscay (Perez-Belmonte, 2008; Delaine  
453 et al., 2015; Arthuis et al., 2015; Arthuis, 2020).

454

455 **5.1.2. “The Turritella layer”: a bio-stratigraphical indicator of the Maximum Flooding**  
456 **Surface establishment**

457 The VK03-58bis core is characterized by a layer showing a high concentration of *Turritella*  
458 *communis* shells (Fig. 3b) and described as the “*Turritella* layer” (TL; Bourillet et al., 2005;  
459 Naughton et al., 2007; Baltzer et al., 2015). In this core, two shells dated at the base (160 cm:  
460 8.4 ka BP) and at the top (149 cm: 7.5 ka BP) of the TL provide a minimal age extension of  
461 900 years for this ~12 cm-thick deposit.

462 Previous studies suggested drastic environmental changes as potential drivers of the TL ending.  
463 First, a potential link between the TL and the abrupt North Atlantic climate shift of the 8.2 ka  
464 BP event was proposed (Naughton et al., 2007; Baltzer et al., 2015). It was then hypothesized  
465 that the North Atlantic sea-surface cooling and related decreasing salinity (Alley et al., 2003)  
466 could have explained the monospecific development of *T. communis* since these taxa are not  
467 sensitive to variations of these hydrological parameters (Funder et al., 2002; Baltzer et al.,  
468 2015). The end of the TL was also attributed to a mortality event induced by the opening of the  
469 English Channel, then contributing to major hydrological and sedimentological changes in the  
470 north-eastern temperate Atlantic Ocean (Naughton et al., 2007). Finally, Baltzer et al. (2015)  
471 suggested that the abrupt sediment supply associated with the rapid RSL rise, and the related  
472 lack of oxygen for benthic organisms, could have been responsible for the *T. communis* death  
473 and burial of their shells.

474 The new AMS-<sup>14</sup>C dates obtained for core VK03-58bis (Table 2) suggest that the TL is related  
475 to extremely low sedimentation rates (~0.01 mm/yr; Fig. 3b) at the end of the TST in the

476 Armorican shelf. In the TL, juvenile and adult specimens are found in a perfect taphonomic  
477 state owing to the absence of broken shells or abrasion marks (*Folliot, 2004; Baltzer et al.*  
478 *2015*). This likely excludes strong bottom energetic currents during the TL interval and suggests  
479 an autochthonous origin and an “*in-situ*” preservation of *T. communis* shells in generally living  
480 position. A winnowing of fine particles (i.e., no observed sandy inputs or specific grain size  
481 distribution) by weak bottom currents may however have occurred, considering the present-day  
482 mud-burrowing mode of life of these filter-feeder gastropods (*Yonge 1946; Carter, 2008*). Both  
483 taphonomic considerations and  $^{14}\text{C}$ -AMS dates therefore argue for a monospecific within-  
484 habitat preservation where fossil assemblages are time-averaged (*Walker and Bambach, 1971;*  
485 *Kidwell, 1997; Fujiwara et al., 2004*), thus implying a succession of several *T. communis*  
486 generations during a long-lasting period (i.e., here ranging between ~1 kyr minimum and 2.1  
487 kyrs maximum) of low sediment supply. We therefore suggest that the TL represents a  
488 condensed level, occurring synchronously with the slower RSL rise rates at the end of the TST.  
489 According to this interpretation, the TL appears as a marker of the MFS in Holocene  
490 transgressive deposits of the Armorican shelf.

491

## 492 **5.2. Palynological records along a proximal-distal gradient during the TST interval** 493 **(8.5–8.3 ka BP)**

494 In the lower part of core MD08-3204 CQ, between 290–196 cm (200 yrs: 8.5–8.3 ka BP),  
495 palynological results (dinocyst and pollen assemblages) were averaged (Fig. 5). In strictly the  
496 same Early Holocene interval, these new palynological data emanating from the inner shelf  
497 (i.e., 0–50 m deep) were compared with previously published data acquired from proximal  
498 coastal to distal marine domains along the Armorican shelf.

499 For this purpose, three cores were selected (Fig. 1a): i) the inner-shelf VC2012-08-PQP core  
500 (PROTEUS-DUNES cruises; *Shom, 2012*) hereafter referred to as core VC-08, retrieved at 28

501 m depth in the shallow coastal Bay of Douarnenez (BD; 17 points extracted from *Lambert et*  
502 *al., 2019*), ii) the mid-shelf VK03-58bis core (Vibarmor cruise; *Le Roy et al., 2003*), retrieved  
503 at 96 m depth in the South Glénan sector of the Grande Vasière (GV; 5 points extracted from  
504 *Naughton et al., 2007* for pollen and *Penaud, pers. comm.* for dinocyst assemblages), and iii)  
505 the distal marine MD95-2002 core (IMAGES 101 expedition; *Bassinot and Labeyrie., 1996*),  
506 retrieved at 2,174 m depth on the Meriadzek Terrace (3 points extracted from *Zumaque et al.,*  
507 *2017* for dinocyst and *Fersi et al., in prep.* for pollen assemblages).

508

### 509 **5.2.1. Averaged 8.5–8.3 ka BP dinocyst observations**

510 From inshore to offshore environments, among a palynomorph sum including pollen grains,  
511 spores, and dinocysts, the dinocyst proportion increases from < 10% in the bays (cores MD08-  
512 3204 CQ and VC-08) to slightly over 50% in the mid-shelf (core VK03-58bis) and offshore  
513 (core MD95-2002) (Fig. 7a). The proximity to the close terrestrial domains, and hence to the  
514 pollinic production sources, appears responsible for the high pollen grain percentages recorded  
515 in the bays (Fig. 7a). A maximum dinocyst diversity is recorded in core VK03-58bis (Fig. 7b),  
516 mainly subjected to oceanic influences at that time (*Penaud et al., 2020*). Dinocyst assemblages  
517 in the two shallowest cores are dominated by inner neritic taxa (i.e., especially *S. bentorii*,  
518 accompanied by *Spiniferites membranaceus*-*Spiniferites belerius*, *Spiniferites delicatus*, and *S.*  
519 *lazus*) that represent a minor part of the assemblage in the mid-shelf and barely occur offshore  
520 (Fig. 7b). Considering the shallow Quiberon and Douarnenez bays, dinocyst assemblages are  
521 consistent with sedimentological studies describing fluvial environments subject to tidal  
522 influences (*Jouet et al., 2003*; *Le Roy and Jouet, 2005*; *Baltzer et al., 2014*; *Gregoire et al.,*  
523 *2017*; *Lambert et al., 2019*). A slight difference is seen among inner neritic assemblages with  
524 major occurrences of *S. bentorii* and cysts of *Pentapharsodinium dalei* in the more enclosed  
525 BD, replaced by *S. lazus* and by the apparition of the neritic group, *Spiniferites ramosus*-

526 *Spiniferites bulloideus*, in the BQ. These assemblages reach their highest values in core VK03-  
527 58bis (Fig. 7b), testifying to their association with peri-Brittany shelf waters (*Morzadec-*  
528 *Kerfourn, 1977; Penaud et al., 2020; Lambert et al., 2022*). In more distal environments,  
529 dinocyst assemblages are mainly composed of outer neritic taxa, especially *S. mirabilis* and *O.*  
530 *centrocarpum*, worthy of note are the unique occurrences of full-oceanic *Impagidinium* species  
531 and the absence of the estuarine *L. machaerophorum* taxon in core MD95-2002 (Fig. 7b). A  
532 steeper marine influence is thus recorded in the distal cores during the Early Holocene, as  
533 recorded during the Mid to Late Holocene (*Penaud et al., 2020*) and in present-day (*Lambert*  
534 *et al., 2022*) dinocyst assemblages along the same inshore-offshore transects.

535

#### 536 **5.2.2. Averaged 8.5–8.3 ka BP pollen observations**

537 During the 8.5–8.3 ka BP interval, a short temporal window during the wider Mesolithic  
538 cultural period (i.e., 10–7 ka BP; 8.5–5.1 ka BC in western Brittany), anthropogenic changes  
539 appear limited, as testified by high arboreal taxa percentages (i.e., 80 to 90% in coastal to mid-  
540 shelf cores) and very low values of anthropogenic taxa (i.e., not exceeding 1%; Fig. 8a). The  
541 high representation of arboreal taxa, related to a still large forest cover on the continent, may  
542 additionally be explained by the pollination period, especially that of *Quercus* whose pollen  
543 grains are present in the atmosphere mainly during spring months (March to June; *Rodríguez-*  
544 *Rajo et al., 2005; García-Mozo et al., 2006*). In a high boreal summer insolation context,  
545 *Penaud et al. (2020)* suggest that the high pollination of trees, coupled with spring to summer  
546 rainfall regimes and related fluvial discharge, could amplify the signature of *Quercus* pollen  
547 grains in the platform, therefore accounting for the highest arboreal pollen fluxes recorded in  
548 the Armorican shelf during the Early Holocene.



549 The more distal marine sequence (i.e., core MD95-2002) is characterized by the highest pollen  
550 diversity and the highest herbaceous percentages when compare with the inshore-offshore  
551 transect (Fig. 8a). The most diverse pollen signature of core MD95-2002 (*Fersi et al., in prep*)  
552 may be explained by the multi-catchment area pollen sources (i.e., macro-regional fluvial  
553 signatures coming from Loire, Gironde, South Brittany, and English Channel watersheds). In  
554 contrast, the two bays imply pollen sources from more limited catchment areas close to the  
555 collected cores (i.e., MD08-3204 CQ at ~5 m depth and VC-08 at ~16 m depth, under a water  
556 column that was 12 m below the present-day sea level; *García-Artola et al., 2018*).  
557 Furthermore, core MD92-2002 presents a unique Cupressaceae signature (including *Juniperus*),  
558 combined with boreal forest taxa (i.e., *Picea-Abies*) and high percentages of the pioneer taxon  
559 *Betula* (Fig 8b), which are likely associated with a northern European continental signature  
560 transported by the English Channel (*Fersi et al., in prep*). In addition, Mediterranean trees  
561 (grouping *Quercus ilex* and *Quercus suber*) are recorded at ~1-2%, in the deep core, but also in  
562 the mid-shelf sequence (i.e., core VK03-58bis; Figs. 8b, c), and may correspond to southern  
563 French river watersheds, implying mainly Loire and to a lesser extent Gironde river influences  
564 (*Penaud et al., 2020*).

565 The pre-6 ka BP interval, still characterized by high RSL rise rates (*García-Artola et al., 2018*)  
566 and the intense activity of the North Atlantic Current (*Ayache et al., 2018*), was described as a  
567 “summer-prevailing mode” in the southern Brittany platform (*Penaud et al., 2020*), i.e., as a  
568 prevalent NW to SE shelf residual circulation in the Bay of Biscay. This prevalent oceanic  
569 influence over the platform may explain the high dinocyst diversity recorded in the mid-shelf  
570 (Fig. 7b). However, the occurrences of Mediterranean tree pollen in the two more distal cores  
571 attest to common continental sources inherited from southern France catchments (Figs. 8b, c).  
572 In the deep MD95-2002 core, the unique occurrences of *Impagidinium* spp.,  
573 *Nematosphaeropsis labyrinthus*, *Brigantedinium* spp. oceanic taxa (Fig. 7b), and Cupressaceae

574 and *Picea-Abies* pollen grains (Figs. 8b, c), indicating rather a distant northern European  
575 continental source carried by oceanic currents that however barely affect the mid-shelf. We  
576 hypothesize that a hydrological front, formed in the northern Bay of Biscay during summer  
577 months, may have prevented the summer transportation of these northern continental sources  
578 to the mid-shelf, while a break of the thermohaline front during winter months may have  
579 favored the transport of southern continental sources up to the northern Bay of Biscay. This  
580 would correspond to the opposite configuration to the one prevailing for the present-day  
581 seasonal hydrological mechanism operating in the Bay of Biscay (i.e., “winter prevailing  
582 mode”, see Fig. 1a), characterized today by the establishment of the thermohaline front during  
583 winter months (*Castaing et al., 1999; Costoya et al., 2016*) and since ~3.3 ka BP (*Mojtahid et*  
584 *al., 2019; Penaud et al., 2020*).

585

### 586 **5.2.3. *Quercus* vs. *Corylus* signature in space and time**

587 Arboreal taxa are dominant along the inshore-offshore transect (Fig. 8a) as commonly observed  
588 and thoroughly discussed in sediment archives (*Broström et al., 2008; Mazier et al., 2008, 2015;*  
589 *Lebreton et al., 2010; Sjögren et al., 2015*). In addition, the anemophilous *Pinus* pollen grains  
590 are over-represented in marine sequences (Fig. 8b) due to their strong capacity of dispersion  
591 (*Turon, 1984; Holmes, 1994*). Excluding *Pinus* and *Picea-Abies* taxa from the arboreal sum  
592 (Fig. 8c), deciduous *Quercus* pollen grain percentages increase from the bays (~same values  
593 for both shallow environments) to the mid-shelf, while those of *Corylus* decrease along this  
594 same gradient. Among the two other temperate forest taxa found in the northern European  
595 sediment archives, we suggest that the *Corylus* signal may decrease with the distance from the  
596 coast, boosting the deciduous *Quercus* expression in more distal sediments (Fig. 8c). This may  
597 explain the fact that the *Corylus* percentages are always higher than the *Quercus* ones,  
598 regardless of the period considered over the last 7 kyrs, in south-western Brittany peat deposits

599 (*Fernane et al., 2014*), whereas the opposite is observed in the southern Brittany coastal  
600 (*Fernane et al., 2015*) and mid-shelf (this study; *Penaud et al., 2020*) environments. In addition,  
601 it should be pointed out that *Quercus* has a high degree of resistance to oxidation (*Lebreton and*  
602 *al., 2010*) that may partly explain its over-representation in marine environments.

603 Moreover, previous studies of the Mid to Late Holocene showed an anti-correlation between  
604 deciduous *Quercus* and *Corylus* pollen percentages, with *Quercus* contractions and *Corylus*  
605 expansions, and *vice-versa*, at a pluri-decadal timescale (*Joly et Visset, 2009; Fernane et al.,*  
606 *2014*). Knowing that *Corylus* pollination takes place during winter months (January to March;  
607 *Bégeot, 1998; Olsen et al., 2000*), contrary to deciduous *Quercus* pollination that occurs during  
608 spring months (March to June; *Rodriguez-Rajo et al., 2005; García-Mozo et al., 2006*),  
609 *Corylus/Quercus* anticorrelations at an infra-orbital timescale could be explained by a stronger  
610 fluvial influence due to enhanced precipitation fostering the *Corylus* signature during the winter  
611 season. In north-western Europe, *Alnus* flowering is very close to that of *Corylus* (*Puc and*  
612 *Kasprzyk, 2013*). A correlation between *Alnus*, and also *Corylus*, and intensified fluvial  
613 discharge is identified in modern sediments from the Bay of Brest (*Lambert et al., 2017*). For  
614 this reason, both *Alnus* and *Corylus* allowed understanding intensified winter paleo-discharge  
615 in the Bay of Brest over the last 2.5 kyrs BP (*Lambert et al., 2020*). In addition, *Penaud et al.*  
616 (*2020*) used the *Corylus/Quercus* ratio over the last 7 kyrs BP (core CBT-CS11 in the southern  
617 Brittany shelf; Fig. 1b) and demonstrated its common trend with alluvial taxa (especially  
618 *Alnus*). From this perspective, *Corylus* (and *Alnus*) vs. *Quercus* pollen percentage fluctuations  
619 detected at a pluri-decadal timescale in Holocene records, may be partly reconciled by  
620 considering periods of enhanced winter precipitation and related fluvial discharge when  
621 *Corylus* percentages increase, and vice versa.

622

623       **5.3. Natural vs. anthropogenic impacts since 5.7 ka BP along an inshore-offshore**  
624               **gradient at the scale of the South Brittany platform**

625 After 5.7 ka BP, in the MD08-3204 CQ core, the resumption of mixed estuarine-marine  
626 sedimentation leads to a continuous palynological record in the BQ. In order to better  
627 understand the paleoenvironmental changes that occurred along the South Brittany coast over  
628 the last 5.7 kyrs BP (at ~100 yrs time resolution), the main palynological results acquired in  
629 this study were selected (i.e., *L. machaerophorum*, *Alnus*, *Corylus*, *Quercus*, Poaceae and API;  
630 orange curves in Figs. 9 and 10). These data are discussed in parallel with two sedimentological  
631 records covering the last 7 kyrs BP (Fig. 2b). First, the mid-shelf CBT-CS11 core (Figs. 1a, b;  
632 CABTEX cruise; *Dussud, 2010*) was acquired at 73 m depth in the south-Penmarc'h sector of  
633 the GV (*Penaud et al., 2020*: ~80 yrs time resolution between 7–0.5 ka BP; blue curves in Figs.  
634 9 and 10). Secondly, the continental GL3 core (*Fernane, 2014*) was retrieved in the South  
635 Brittany coastal wetland of Guidel (Figs. 1a, b) and corresponds to an ancient ria progressively  
636 transformed into a maritime coastal marsh during the Holocene transgression (*Fernane et al.,*  
637 *2015*: ~85 yrs time resolution between 7–0.6 ka BP; green curves in Figs. 9 and 10).

638

639       **5.3.1. Fluvial hydrosystem processes and related shelf sedimentation**

640 Dinocyst data acquired in the BQ over the last 5.7 kyrs BP show a clear dominance of *L.*  
641 *machaerophorum*, that started to increase at ~5.9 ka BP according to the 7 kyr-long CBT-CS11  
642 core (*Penaud et al., 2020*; Fig. 9). This species is tolerant to large drops in salinity and is well  
643 known to proliferate in brackish environments (*Reid, 1975*; *Morzadec-Kerfourn, 1977, 1992,*  
644 *1997*). At the same time, pollen grains of the riparian taxon *Alnus*, a hydrophilous tree  
645 developing mainly along freshwater bodies, reaches its maximum values in both MD08-3204  
646 CQ and CBT-CS11 cores (Fig. 9). The 5.7 ka BP limit corresponds to the major inflection in

647 the RSL rise rates occurring at ~6 ka BP (*Goslin et al., 2015; Stéphan et al., 2015; García-*  
648 *Artola et al., 2018*), then corresponding to the stabilization of fluvial systems (*Penaud et al.,*  
649 *2020*). The riparian vegetation (i.e., *Alnus*) then progressively colonizes coastal marshes, which  
650 in turn promotes the fixation of vegetation in riverbanks and valley alluviation (*Penaud et al.*  
651 *2020*). The increase in estuarine-sensitive taxa (i.e., *Alnus* and *L. machaerophorum*; Fig. 9) in  
652 coastal areas argues for a stronger fluvial influence on the shelf since 5.7 ka BP, which is  
653 consistent with the HST establishment (subsection 5.1.1). The typical neritic dinocyst  
654 assemblage, obvious during the TST configuration, appears extremely different when  
655 considering dinocyst percentages after 5.7 ka BP that are characterized by the over-  
656 representation of *L. machaerophorum* (mean of 83%; Fig. 6). However, if *L. machaerophorum*  
657 is excluded from the main sum, dinocyst percentages appear quite similar to the pre-5.7 ka BP  
658 period (Fig. 6). This argues for an allochthonous signal of the estuarine-sensitive taxon *L.*  
659 *machaerophorum*, likely carried to the Armorican shelf by main river discharge, especially the  
660 Loire and Vilaine rivers (Fig. 6). Furthermore, *Delaine et al. (2015)* examined the Holocene  
661 sediment infilling of the upstream Loire Valley and recorded a high erosional regime of the  
662 Loire system between ~5.8–2.1 ka BP in a context when sedimentation rates exceeded the RSL  
663 rise rates. This may have led to a shift of the sediment depo-center towards the Armorican shelf,  
664 as testified by the coarser sedimentation recorded in core CBT-CS11 up to ~3.3 ka BP  
665 (*Mojtahid et al., 2019; Penaud et al., 2020*; D50 CaCO<sub>3</sub> free in Fig. 9). After 3.3 ka BP, the  
666 decrease of estuarine-sensitive taxa (i.e., *Alnus*, *Corylus* and *L. machaerophorum*) percentages  
667 and sediment grain-size values recorded in core CBT-CS11 (Fig. 9) suggest a decreasing  
668 influence of the paleo-Loire erosional dynamics. Geomorphological studies have shown that  
669 the sediment load may have exceeded the transport capacity leading to a Loire riverbed  
670 elevation at ~2.7 ka BP (*Castanet, 2008; Arthuis, 2020*). The progressive infilling of the

671 estuarine system contributed to the decrease of the river slope and likely also the load-transport  
672 capacity of the Loire river at ~3 ka BP.

673 In contrast, in core MD08-3204 CQ, estuarine-sensitive taxa percentages remain quite constant  
674 around 3 ka BP (Fig. 9). This may be explained by the location of the BQ, semi-isolated by the  
675 Quiberon peninsula and islands (*Houat, Hoedic and Belle-Ile*; Fig. 1b), then exposed to the  
676 additional influences of the Gulf of Morbihan and Bay of Vilaine fluvial sediment supply  
677 (*Menier et al., 2010, 2014*). At that time, the Vilaine river dynamics (different from the Loire  
678 river ones) may have maintained the sediment load to the platform in the BQ. It is worth noting  
679 that the Vilaine fluvial system has now been totally altered since the construction of the Arzal  
680 dam in 1970, reducing water fluxes (~71 m<sup>3</sup>/s between 1970 and 2000 in Rieux,  
681 [www.hydro.eaufrance.fr](http://www.hydro.eaufrance.fr)) and thus sediment transfers to the platform, which are therefore no  
682 longer comparable today to the above-described Late Holocene discussion for the BQ. After  
683 2.4 ka BP, the decline of the general forest cover (i.e., *Alnus, Quercus, Corylus*; Fig. 9) is  
684 accompanied by an increase in Poaceae and Anthropogenic Pollen Indicators (API; Figs. 9 and  
685 10), testifying to the continentalization of the coastal environment under the strong human-  
686 forced influence on freshwater bodies (*Delaine et al., 2015*).

687

### 688 ***5.3.2. The anthropogenic pollen signature along the South Brittany coast***

689 The continental core GL3 (*Fernane et al., 2015*) provides a local anthropogenic signal restricted  
690 to southern Brittany watersheds, whereas the two shelf cores CBT-CS11 (*Penaud et al., 2020*)  
691 and MD08-3204 CQ (this study) provide a more regional averaged anthropogenic signal at the  
692 scale of western French watersheds involving Loire, Vilaine and southern Brittany rivers (Fig.  
693 1b).

694 In our study, during the Neolithic interval (7–4.2 ka BP / 5–2.2 ka BC), arboreal taxa  
695 percentages (especially *Quercus*) remain high in the two shelf sequences, whereas in the  
696 continental site of Guidel, sharp fluctuations affect the arboreal trend (i.e., *Quercus* and  
697 *Corylus*) and are explained mainly by recurrent increases in Poaceae percentages (Fig. 9). In  
698 this site, the anthropogenic activity is confirmed by co-occurrences of ruderal and adventitious  
699 taxa and discrete occurrences of cultivated plants, occurring mainly in the 6.4–5.1 ka BP  
700 interval (/4.4–3.1 ka BC; Fig. 10c; *Fernane et al., 2015*). Along the South Brittany coast, several  
701 continental palynological studies (*Visset et al., 1996; Gaudin, 2004; Visset and Bernard, 2006*)  
702 attest to Neolithic agro-pastoral activities with sporadic *Cerealia*-type occurrences. On land,  
703 the anthropogenic signal is captured by small sedimentary basins, such as the coastal wetland  
704 of Guidel. Although deforestation and agro-pastoral practices are well-referenced on land,  
705 ruderal and adventitious taxa remain low in shelf cores with no co-occurrences of cultivated  
706 taxa (Figs. 10a, b). We suggest that during the Mid-Holocene, Poaceae and API, already weakly  
707 recorded far from emission sources, are insufficiently transmitted to the platform to be  
708 significantly recorded in marine sediments.

709 From 4.2 ka BP (i.e., the start of the Late Holocene from a stratigraphical point of view; *Walker*  
710 *et al., 2019*), a major reorganization affects oceanic and atmospheric dynamics, as recently  
711 discussed at the Bay of Biscay scale (*Penaud et al., 2020*). The winter insolation at 65°N  
712 increases along the Holocene favoring wetter and milder winters over northern Europe (*Benito*  
713 *et al., 2015*). The intensification of a winter precipitation regime led to enhanced river  
714 discharge, as shown by the high percentages (Figs. 5a and 6) and fluxes (Fig. 6) of *L.*  
715 *machaerophorum*. Subsequently, higher river discharge led to the establishment of the winter  
716 thermohaline front at ~3.3 ka BP along the BoB (*Mojtahid et al., 2019; Penaud et al., 2020*).  
717 This configuration enhanced the transmission of the API signature from the watersheds to  
718 coastal waters. From 4.2 ka BP (/2.2 ka BC), and across the Bronze and Iron Ages (4.2–2 ka

719 BP / 2.2 ka BP–50 BC), all sequences point to a synchronous arboreal percentage decrease,  
720 together with the progressive increase in Poaceae percentages (Fig. 9). From this boundary, the  
721 two shelf sequences show an apparent discontinuous record related to the rise of API  
722 percentages (i.e., adventitious, ruderal and cultivated taxa; Figs. 10a, b), whereas the rise in API  
723 percentages is continuous from 3.3 ka BP at Guidel (Fig. 10c). This palynological trend  
724 confirms the major human-induced landscape transformation that occurred under enhanced  
725 agro-pastoral activities discussed with archeological (*Pailler and Nicolas, 2019*) and  
726 continental palynological (*Marguerie, 1990, 1992, 1993; Gaudin, 2004; van Beek et al., 2018*)  
727 data. In Guidel, a second major shift in terms of human impact, highlighted by the sharp drop  
728 of arboreal taxa and the related increase of Poaceae percentages (Fig. 9), occurs at around 2.4  
729 ka BP (/450 BC), i.e., at the second Iron Age. In all sequences, the API signature tends to  
730 increase at ~1.2 ka BP (Fig. 10). At that time, the maximum percentages of cultivated taxa are  
731 due to the intensification and diversification of agriculture practices in western France  
732 (*Marguerie, 1992; Visset et al., 1995; Gaudin, 2004; Fernane et al., 2015*), showing the massive  
733 opening of the landscape and foreshadowing the present-day bocage organization of the area  
734 (*Barbier, 1999; Cyprien, 2002; Marguerie, 2003*).

735

### 736 ***5.3.3. Impact of multi-secular hydro-climatic forcing on the Anthropogenic Pollen*** 737 ***Indicator (API) record***

738 Guidel (continental, core GL3) and Quiberon (protected shelf, core MD08-3204 CQ)  
739 environmental contexts are mainly associated with South Brittany watersheds (Fig. 1b).  
740 Furthermore, cores MD08-3204 CQ and CBT-CS11 (Fig. 1b) are exposed to additional input  
741 from the Loire River especially since the stabilization of the sea level at ~6 ka BP and the  
742 subsequent increase of winter fluvial discharge at 4.2. ka BP (subsection 5.3.1.). It is thus  
743 possible to compare and discuss these three cores as end-members in terms of continental



744 sources with South Brittany proximal inputs (i.e., Laïta River influence; Fig. 1a) for core GL3,  
745 Loire River for core CBT-CS11, and mixed river sources for core MD08-3204 CQ.

746 In core GL3, the increase in API percentages is obvious across the intervals 6.4–5.1, 3.3–2.7  
747 and 1.6–1.2 ka BP (grey bands in Fig. 10), identified in *Penaud et al. (2020)* as periods  
748 characterized by enhanced subpolar gyre (SPG) strength at times of Bond events 4, 2 and 1,  
749 respectively (*Bond et al., 1997, 2001*). These API increases are also observed in core MD08-  
750 3204 CQ, except for the 6.4–5.1 ka BP interval that corresponds to a Mid-Holocene period  
751 when we argue for a less continental influence and therefore a lower API transmission to the  
752 platform (subsection 5.3.2.). General intensification of anthropogenic activities during these  
753 three intervals was not recorded in previous continental studies (*Visset et al., 1995, 1996*;  
754 *Gaudin, 2004*; *Visset and Bernard, 2006*; *van Beek et al., 2018*). Regarding core CBT-CS11,  
755 the API signal seems to show an opposite behavior, although the anthropogenic history of the  
756 Loire watersheds is not opposite to that of the South Brittany ones. The palynological data  
757 acquired on this mid-shelf core were previously discussed in the context of a millennial-scale  
758 mechanism implying SPG strength coupled with natural atmospheric oscillations (*Penaud et*  
759 *al., 2020*). In this model, North Atlantic gyre responses are supposed to be strongly related to  
760 persistent North Atlantic Oscillations (NAO) configurations, even though a large non-linearity  
761 exists today regarding gyre responses to the atmospheric forcing (*Lohmann et al., 2009*). Hence,  
762 stronger Loire river discharge would represent a conjectural phenomenon of weakened SPG  
763 influence under recurrent negative NAO-like modes (*Benito et al., 2015*). This would explain  
764 a higher transmission of the API signal to the mid-shelf (core CBT-CS11) outside the Bond  
765 events (higher API amplitudes in between the grey bands identified in Fig. 10a). This model  
766 appears consistent with the stronger API detection observed in core GL3 (Fig. 10c) during  
767 periods of enhanced SPG, in a general context of the northern location of the westerly storm  
768 tracks (*Giraudeau et al., 2010*; *Goslin et al., 2018*; *Lambert et al., 2020*; *Penaud et al., 2020*)

769 with related increases of winter precipitation and fluvial discharge over northern Europe  
770 (*Hurrell, 1995; Hurrell et al., 2003; Tréguer et al., 2014*). Interestingly, it appears that the BQ  
771 could be compared to the observations made at Guidel, with however a less clear-cut API  
772 signature (Fig. 10b). From 5.7 ka BP, the BQ thus appears as a pivotal zone characterized by a  
773 stronger diversity of continental inputs related to different forcing also implying climate  
774 regimes at an infra-orbital timescale previously discussed and better expressed with core CBT-  
775 CS11.

776 Then, from 1.2 ka BP (/ 750 AD), in all cores the anthropogenic influence is characterized by  
777 highest amplitude peaks (Fig. 10). This boundary, corresponding to the start of the Middle Ages,  
778 appears as a limit from which anthropogenic forcing may outweigh the natural climate  
779 variability at the sub-orbital timescale.

780

## 781 6. Conclusion

782 Various factors forced coastal paleoenvironmental changes and palynological records during  
783 the Holocene, including the Relative Sea Level (RSL) rise that modified sedimentation  
784 processes, the fluvial discharge affected by both atmospheric and oceanic dynamics, and the  
785 anthropogenic impact. The present study examines Holocene paleoenvironmental changes  
786 along the Armorican shelf through a compilation of previously published and recently acquired  
787 data. First, new chronostratigraphies of the inner shelf MD08-3204 CQ (Bay of Quiberon, BQ)  
788 and mid-shelf VK03-58bis (Grande Vasière, GV) cores allowed refining the sedimentation  
789 model of the Armorican shelf. In addition, the new palynological (pollen and dinocyst) data  
790 acquired in core MD08-3204 CQ complete a set of pre-existing data acquired from the  
791 continental to the mid-shelf domains. This comparative approach has brought about a synthesis  
792 of the major environmental and hydrological reorganizations that affected the Armorican shelf  
793 over the last 10 kyrs BP:

- 794 • *From 10 to 8.3 ka BP.* The still strong Early Holocene RSL rise rates are responsible  
795 for the high sedimentation (~4.5 mm/yr in the BQ and ~0.66 mm/yr in the GV) rates  
796 leading to the Transgressive System Tract (TST) establishment over the Armorican  
797 shelf.
- 798 • *From 8.3 to 5.7 ka BP.* The slowdown of the RSL rise rates leads to a reduced  
799 accommodation space and to sedimentary remobilization in the BQ. In the GV, the  
800 condensed level corresponding to the already know “*Turritella* layer” is now  
801 identified between 8.4 and 6.3 ka BP, and appears as a biostratigraphical marker of  
802 the Maximum Flooding Surface (MFS) establishment in the Holocene sediments of  
803 the Armorican shelf.
- 804 • *From 5.7 to 3.3 ka BP.* The RSL slowdown and the reduced accommodation space,  
805 bringing low sedimentation rates (~0.24 mm/yr in the BQ and ~0.22 mm/yr in the

806 GV), led to the establishment of the Highstand System Tract (HST). As evidenced  
807 by the rise of estuarine-sensitive taxa (i.e., *Alnus* and *L. machaerophorum*), the  
808 fluvial influence, mainly from the Loire river whose load-transport capacity remains  
809 important, is growing on the platform.

810 • *From 3.3 to 2.4 ka BP.* The Loire River transport capacity declines, leading to a  
811 decrease in the erosive dynamics of the paleo-Loire. At that time, a different hydro-  
812 sedimentary dynamic of the Vilaine River likely maintained a high sediment load  
813 over the BQ.

814 • *Since 2.4 ka BP.* A continentalization of coastal ecosystems is widely recorded.  
815 Increases of both human activities and fluvial influences provide for a better  
816 transport of Anthropogenic Pollen Indicators (API), then better recorded over the  
817 platform, especially from 1.2 ka BP at the start of the Middle Ages.

818 By comparing multiple palynological sequences, located from onshore to offshore domains, our  
819 study also demonstrates the complexity of the API record during the Mid to Late Holocene. We  
820 suggest that the intensification of the fluvial discharge over the South Brittany watersheds  
821 during periods of subpolar gyre (SPG) strengthening tends to enhance continental palynomorph  
822 fluxes, particularly API, in Brittany coastal domains. Conversely, a weakened SPG associated  
823 with an intensified winter precipitation regimes over southern Loire catchments would tend to  
824 increase the API detection on the mid-shelf. In conclusion, at an infra-orbital timescale, the API  
825 signal detected in shelf sediments appears strongly connected to the hydro-climatic control on  
826 precipitation and related fluvial discharge. Without a fine understanding of all forcing  
827 parameters, discussing human dynamics from marine sediments would be biased by natural  
828 controls that deserve to be deconvoluted as a first step.

829

## 830 **7. Acknowledgments**

831 This work was part of a PhD thesis (Ophélie David) financed by the UBS (Univ. Bretagne Sud)  
832 and UBO (Univ Brest). We thank captains, crews, and scientific teams of the different cruises  
833 that collected both main study cores: the MD08-3204 CQ core (BISCOT campaign onboard the  
834 *Marion Dufresne*; MD169/MICROSYSTEMS cruise, 2008; IPEV) and the VK03-58bis core  
835 (Ifremer research project “*Défi Golfe de Gascogne*”; Vibarmor cruise, 2003 onboard the *Côtes*  
836 *de la Manche*). For the other cores discussed in the manuscript, we are indebted to the research  
837 projects involved in core retrieval and data acquisition (1) CBT-CS11 core (in *Penaud et al.*,  
838 2020); CABTEX cruise by the Ifremer onboard the R/V *Pourquoi Pas?* (*Dussud, 2010*); CNRS-  
839 INSU project HCOG2 (2013-2014) and ANR “HAMOC”; 2) VC2012-08-PQP core (in  
840 *Lambert et al., 2019*); PROTEUS-DUNES cruises; *Shom, 2012*; 3) GL3 core (in *Fernane et*  
841 *al., 2015*); ANR “COCORISCO”, Brittany region project “PHILTRE”; 4) MD95-2002 core (in  
842 *Zumaque et al., 2017*); IMAGES 101 expedition; *Bassinot and Labeyrie (1996)*; ANR  
843 “HAMOC”.

844 The palynological analysis of core VK03-58bis received fundings from a CNRS-INSU project  
845 HCOG2 (2013-2014) “*Forçages climatiques Holocène et répercussions Côtières et Océaniques*  
846 *dans le Golfe de Gascogne*” (coord. A. Penaud) as part of the LEFE-IMAGO research program.  
847 We thank Muriel Georget (EPOC; Univ. Bordeaux) and Pierre-Olivier Coste (Geo-Ocean,  
848 Univ. Brest) for their palynological laboratory assistance for the VK03-58bis and MD08-3204  
849 CQ cores, respectively. To the QUIPALPLO project (coord. A. Baltzer), financed by OSUNA  
850 (Observatoire des Sciences de l’Univers de Nantes Atlantique), made possible some  
851 palynological analyses realized during the M2 internship of M. Herlédan (2019/2020). Some  
852 dates were obtained thanks to the French ARTEMIS <sup>14</sup>C-AMS platform, and the others were  
853 acquired at the Poznań Radiocarbon Laboratory and Beta Analytics. We are also grateful to  
854 Anne Véronique Walter-Simonnet (UMR 6249 Chrono-environnement; Univ. Bourgogne

855 Franche-Comté) who carried out the grain size, calcimetry, and TOC analyses of core MD08-  
856 3204 CQ. The authors are grateful to the ZABrI (“*Zone Atelier Brest Iroise*”, CNRS-INEE) and  
857 the ArMeRIE program funded by the UBO (Univ Brest) for fruitful interdisciplinary exchanges  
858 about human dynamics and Holocene paleoenvironments. This work was supported by the  
859 ISblue project (Interdisciplinary graduate school for the blue planet, ANR-17-EURE-0015), co-  
860 funded by a grant from the French government under the program "Investissements d'Avenir".

861

## 862 **8. Data availability**

863 All the data acquired on cores MD08-3204 CQ and VK03-58 bis, and discussed in the  
864 manuscript are available in the SEANOE repository: <https://doi.org/10.17882/86430>

865

866 **9. Table captions**

867 **Table 1:** MD08-3204 CQ AMS-<sup>14</sup>C dates. In grey: dates previously published in *Baltzer et al.*  
 868 (2014). In black: new dates from this study acquired at the Poznań Radiocarbon Laboratory  
 869 (Poz-x) and ARTEMIS (SacA x). All AMS-<sup>14</sup>C dates were calibrated with the CALIB 7.1  
 870 software using the IntCal20 calibration curve (*Stuiver and Reimer, 1993; Reimer et al., 2020*),  
 871 first considering a reservoir age of  $-400 \pm 45$  years to radiocarbon dates (point 1559 for the  
 872 lower Loire in the marine20 database; *Tisnérat-Laborde et al., 2010*).

873

Code	Depth (cm)	Sample nature	Age <sup>14</sup> C BP ± error		Age min (mean) max Cal BP
<i>Lyon 6307</i>	20	<i>Turritella communis</i>	1510	30	955 ( <b>1011</b> ) 1067
Poz-113445	35	<i>Turritella communis</i>	2355	30	1820 ( <b>1884</b> ) 1948
<i>Poz-33086</i>	47	<i>Turritella communis</i>	2745	35	2312 ( <b>2400.5</b> ) 2489
Poz-113447	70.5	Bivalve	3585	30	3361 ( <b>3407.5</b> ) 3454
<i>Poz-33089</i>	79	<i>Turritella communis</i>	3850	40	3616 ( <b>3724</b> ) 3832
<i>Poz-26298</i>	93	<i>Turritella communis</i>	4190	35	4082 ( <b>4187</b> ) 4292
Poz-117547	111	Shell debris	4755	35	4847 ( <b>4913.5</b> ) 4980
Poz-113448	134	Gastropod	5420	35	5657 ( <b>5776</b> ) 5895
Poz-117549	152	Shell debris	5095	35	5320 ( <b>5400</b> ) 5480
Poz-117550	196	Bivalve	7960	40	8350 ( <b>8375.5</b> ) 8401
SacA 29329	225	Shell debris	8060	40	8386 ( <b>8462.5</b> ) 8539
SacA 29330	231	Shell debris	8160	45	8422 ( <b>8511.5</b> ) 8601
SacA 54334	235.5	Gastropod	8145	35	8442 ( <b>8517</b> ) 8592
SacA 32028	241.5	Gastropod	8025	30	8385 ( <b>8403.5</b> ) 8422
Poz-113449	287	Gastropod	8210	50	8429 ( <b>8576.5</b> ) 8724

874

875 **Table 2:** VK03-58bis AMS-<sup>14</sup>C dates. In grey: dates previously published in *Naughton et al.*  
876 (2007). In black: new dates from this study acquired at the Poznań Radiocarbon Laboratory  
877 (Poz-x), ARTEMIS (SacA x), and Beta Analytics (BETA-x). All AMS-<sup>14</sup>C dates were  
878 calibrated with the CALIB 7.1 software using the IntCal20 calibration curve (*Stuiver and*  
879 *Reimer, 1993; Reimer et al., 2020*), first considering a reservoir age of  $-400 \pm 45$  years to  
880 radiocarbon dates (point 1559 for the lower Loire in the marine20 database; *Tisnérat-Laborde*  
881 *et al., 2010*).

882

Code	Depth (cm)	Sample nature	Age <sup>14</sup> C BP ± error		Age min (mean) max Cal BP
Poz-47041	32	Benthic foraminifera	2005	30	1408 ( <b>1471.5</b> ) 1535
Poz-47042	57	Benthic foraminifera	2810	70	2340 ( <b>2526.5</b> ) 2713
Poz-47043	92	Benthic foraminifera	3930	30	3714 ( <b>3760</b> ) 3806
<i>Poz-10166</i>	106	<i>Turritella communis</i>	3820	30	3572 ( <b>3647.5</b> ) 3723
SacA55613	110	<i>Turritella communis</i>	4110	30	3974 ( <b>4038</b> ) 4102
BETA-550086	125	Benthic foraminifera	5410	30	5653 ( <b>5710</b> ) 5767
Poz-47044	137	Benthic foraminifera	5940	40	6280 ( <b>6341</b> ) 6402
SacA55614	140	<i>Turritella communis</i>	7295	30	7678 ( <b>7712.5</b> ) 7747
<i>Poz-10167</i>	149	<i>Turritella communis</i>	7020	40	7431 ( <b>7476.5</b> ) 7522
<i>Poz-10168</i>	160	<i>Turritella communis</i>	8030	40	8369 ( <b>8444.5</b> ) 8520
<i>Poz-10170</i>	177	<i>Turritella communis</i>	8170	40	8429 ( <b>8515.5</b> ) 8602
BETA-550087	179	Benthic foraminifera	7900	30	8321 ( <b>8347</b> ) 8373
BETA-550088	210	Benthic foraminifera	8940	30	9486 ( <b>9414.5</b> ) 9543
<i>Poz-10171</i>	226	<i>Turritella communis</i>	8240	40	8521 ( <b>8648</b> ) 8775
BETA-550089	266	Benthic foraminifera	9400	40	10170 ( <b>10201</b> ) 10235

883



884 **Table 3:** This table gathers core MD08-3204 CQ data discussed in this study and describes the  
 885 methodology used to calculate palynological relative abundances, absolute concentrations, and  
 886 indexes, as well as dinocyst and pollen groups made according to ecological affinities (*Peñaud*  
 887 *et al., 2020*).

888

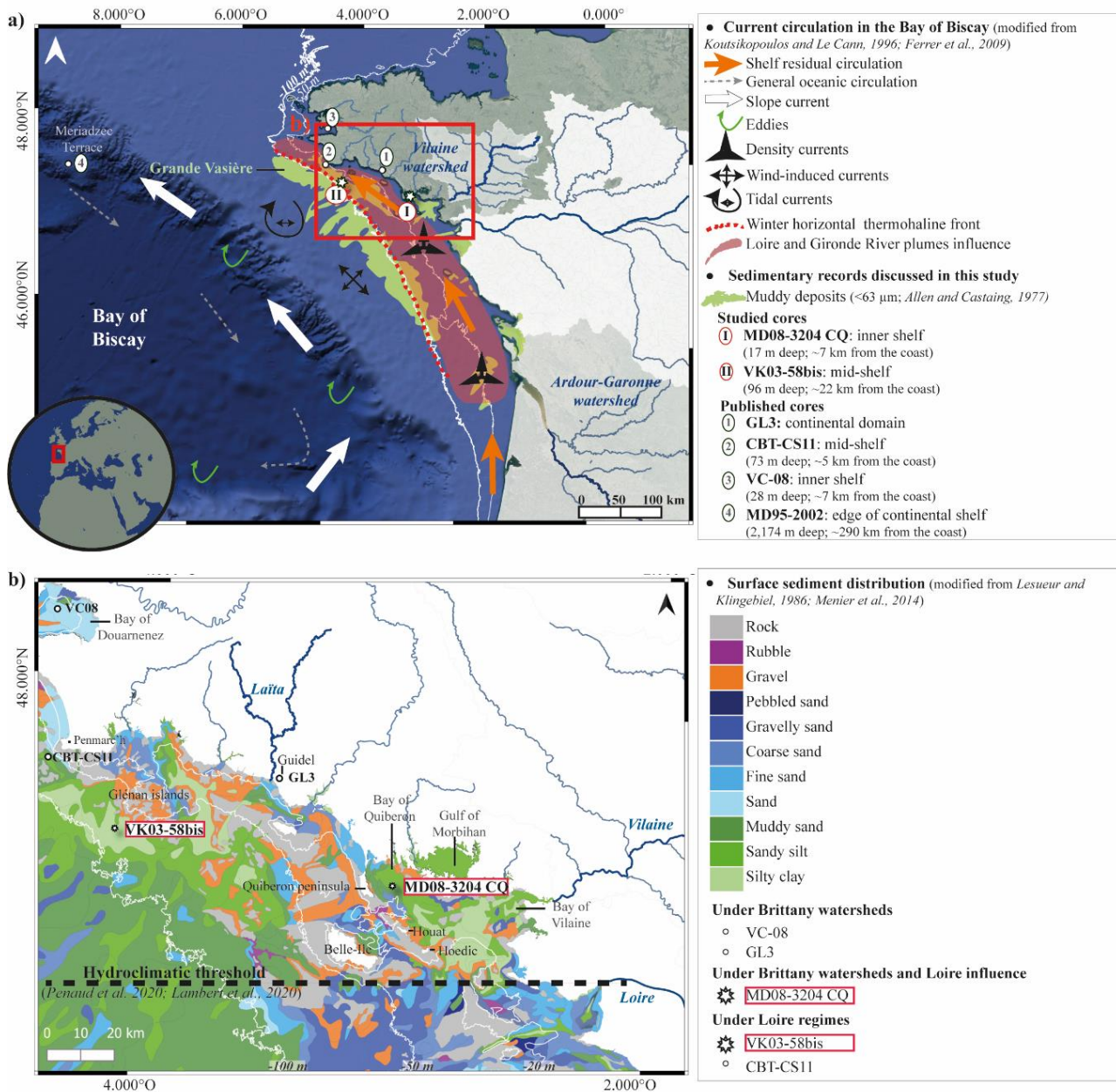
	MD08-3204 CQ data	METHODOLOGY
PALYNOLOGICAL REPRESENTATION	<b>Palynomorph relative abundances (%)</b>	Pollen percentages are calculated using a main sum excluding i) <i>Pinus</i> counts ( <i>Pinus</i> pollen grains thus always tend to be over-represented in marine sediments due to better dispersal and conservation), ii) spores and iii) indeterminable pollen grains. Dinocyst percentages are calculated on a sum of total dinocysts excluding pre-Quaternary specimens.
	<b>Palynomorph absolute concentrations (taxa/cm<sup>3</sup>)</b>	Palynomorph concentrations are based on the marker grain method with <i>Lycopodium</i> spores (de Vernal et al., 1999; Mertens et al., 2009); calibrated tablets of known numbers of spores (here 28 848) being added to each sample before chemical treatments.
	<b>Diversity (Margalef) index</b>	$(S-1)/\ln(n)$ where S is the number of taxa per sample and n is the number of individuals (pollen grains or dinocysts) counted in each sample.
	<b>Dominance index</b>	Dominance ranges from 0 (all taxa are equally present) to 1 (one taxa dominates the assemblage). Dominance=1-Simpson index.
	<b>Taxon richness</b>	Number of different taxa present in each analyzed level
DINOCYST GROUPS	<b>Sum inner neritic taxa (Cysts of phototrophs or mixotrophs)</b>	<i>Spiniferites bentorii</i> (Sben), <i>Spiniferites lazus</i> (Slaz), <i>Spiniferites membranaceus</i> (Smem), <i>Spiniferites belerius</i> (Sbel), <i>Spiniferites delicatus</i> (Sdel), <i>Spiniferites ristingensis</i> (Sris), Cysts of <i>Protoperidinium dalei</i> (Pdai)
	<b>Sum outer neritic taxa (Cysts of phototrophs or mixotrophs)</b>	<i>Spiniferites ramosus</i> (Sram) / <i>Spiniferites bulloideus</i> (Sbul), <i>Operculodinium centrocarpum</i> sensu Wall & Dale, 1966 (Ocen), <i>Spiniferites mirabilis</i> (Smir)
	<b>Sum inner neritic taxa (Cysts of heterotrophs)</b>	Cysts of <i>Protoperidinium nudum</i> (Pnud) / <i>Selenopemphix quanta</i> (Squa), Cysts of <i>Protoperidinium stellatum</i> (Pste), <i>Xandarodinium xanthum</i> (Xand)
POLLEN GROUPS	<b>Sum AP (arboreal taxa)</b>	<u>Major taxa &gt;2%:</u> <i>Quercus</i> , <i>Corylus</i> , <i>Hedera</i> , <i>Betula</i> , <i>Ulmus</i> , <i>Tilia</i> , <i>Fagus</i> <u>Minor taxa &lt;2%:</u> <i>Ilex</i> , <i>Carpinus</i> , <i>Prunus</i> , <i>Populus</i> , <i>Taxus</i> , <i>Abies</i> , <i>Viburnum</i> , <i>Juniperus</i> , <i>Ribes</i>
	<b>Sum riparian trees</b>	<u>Major taxa &gt;2%:</u> <i>Alnus</i> , <i>Salix</i> , <i>Fraxinus</i>
	<b>Non-indigenous trees</b>	<u>Major taxa &gt;2%:</u> <i>Castanea</i> <u>Minor taxa &lt;2%:</u> <i>Vitis</i> , <i>Quercus ilex</i> , <i>Buxus</i> , <i>Juglans</i>
	<b>Sum NAP (herbaceous taxa)</b>	<u>Major taxa &gt;2%:</u> Poaceae, Chenopodiaceae, Asteroideae, Brassicaceae, Cichorioideae, Cyperaceae, Ericaceae, <i>Lotus</i> , Juncaceae, <i>Plantago coronopus</i> , <i>Plantago</i> spp., Primulaceae, Ranunculaceae, <i>Saxifraga</i> <u>Minor taxa &lt;2%:</u> <i>Sagittaria</i> , Amaryllidaceae, Apiaceae, Boraginaceae, Campanulaceae, <i>Centranthus</i> , <i>Spergula/Spergularia</i> , Caryophyllaceae, <i>Cistus</i> , <i>Sedum</i> ,

	Crassulaceae, <i>Ephedra</i> , Euphorbiaceae, <i>Trifolium</i> , <i>Ulex</i> , Fabaceae, Gentianaceae, Geraniaceae, <i>Myriophyllum</i> , Iridaceae, <i>Lemna</i> , Liliaceae, <i>Papaver</i> , <i>Plantago maritima</i> , <i>Veronica</i> , <i>Armeria</i> , <i>Limonium</i> , <i>Potamogeton</i> , Oenotheraceae, Rosaceae, <i>Euphrasia</i> , Scrophulariaceae, <i>Typha/Sparganium</i> , Rubiaceae, <i>Viola</i> , <i>Hypericum</i> , <i>Polygonum</i> , Lamiaceae, <i>Althaenia</i> , <i>Helianthemum</i> , <i>Matthiola</i> , <i>Convolvulus</i>
<b>Sum ruderal and adventives</b>	<u>Major taxa &gt;2%</u> : <i>Rumex</i> , <i>Artemisia</i> , <i>Plantago lanceolata</i> <u>Minor taxa &lt;2%</u> : <i>Mercurialis</i> , <i>Centaurea</i> , <i>Papaver</i> , Urticaceae
<b>Sum cultivated taxa</b>	<u>Major taxa &gt;2%</u> : <i>Cerealia</i> -type <u>Minor taxa &lt;2%</u> : Cannabaceae

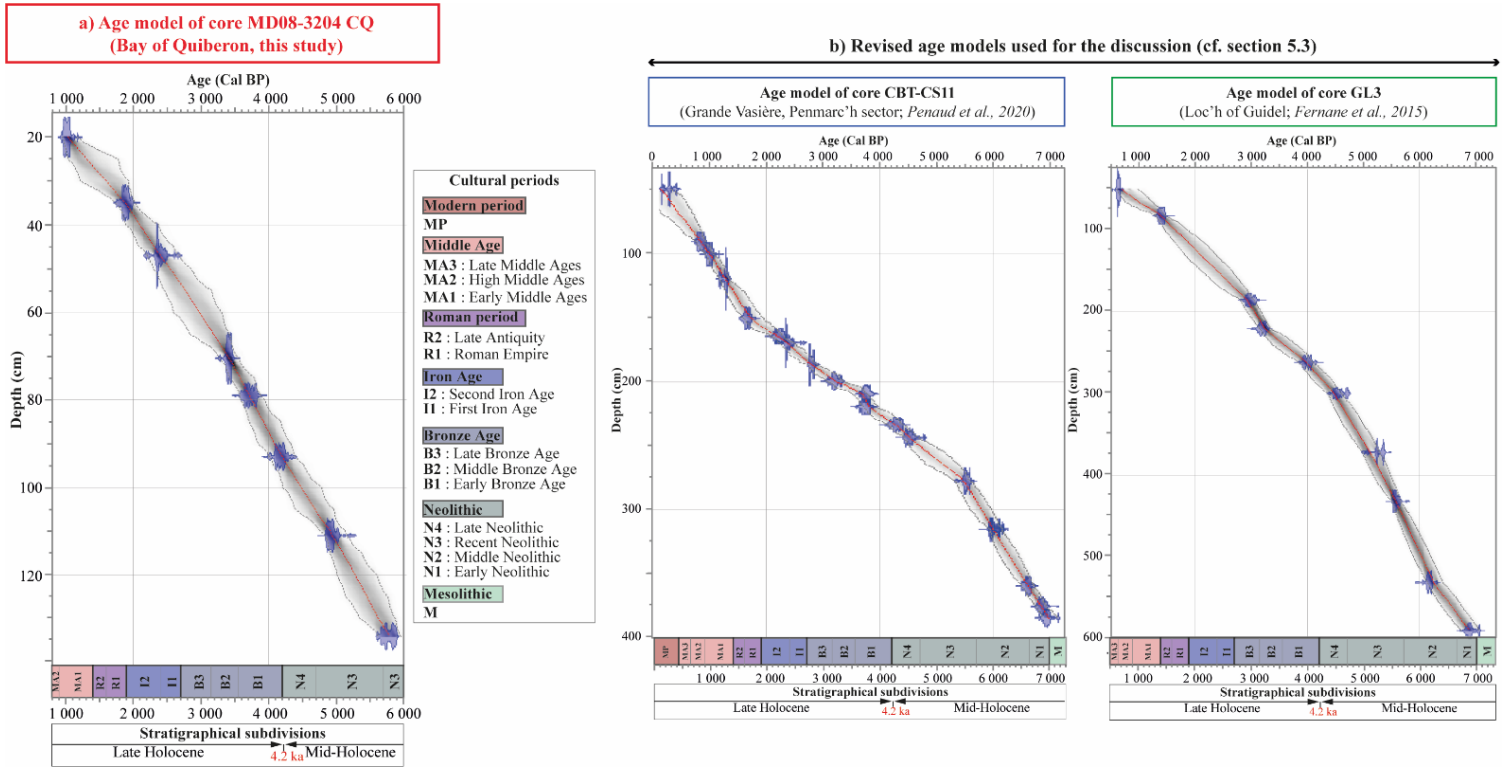
889

890 **10. Figure captions**

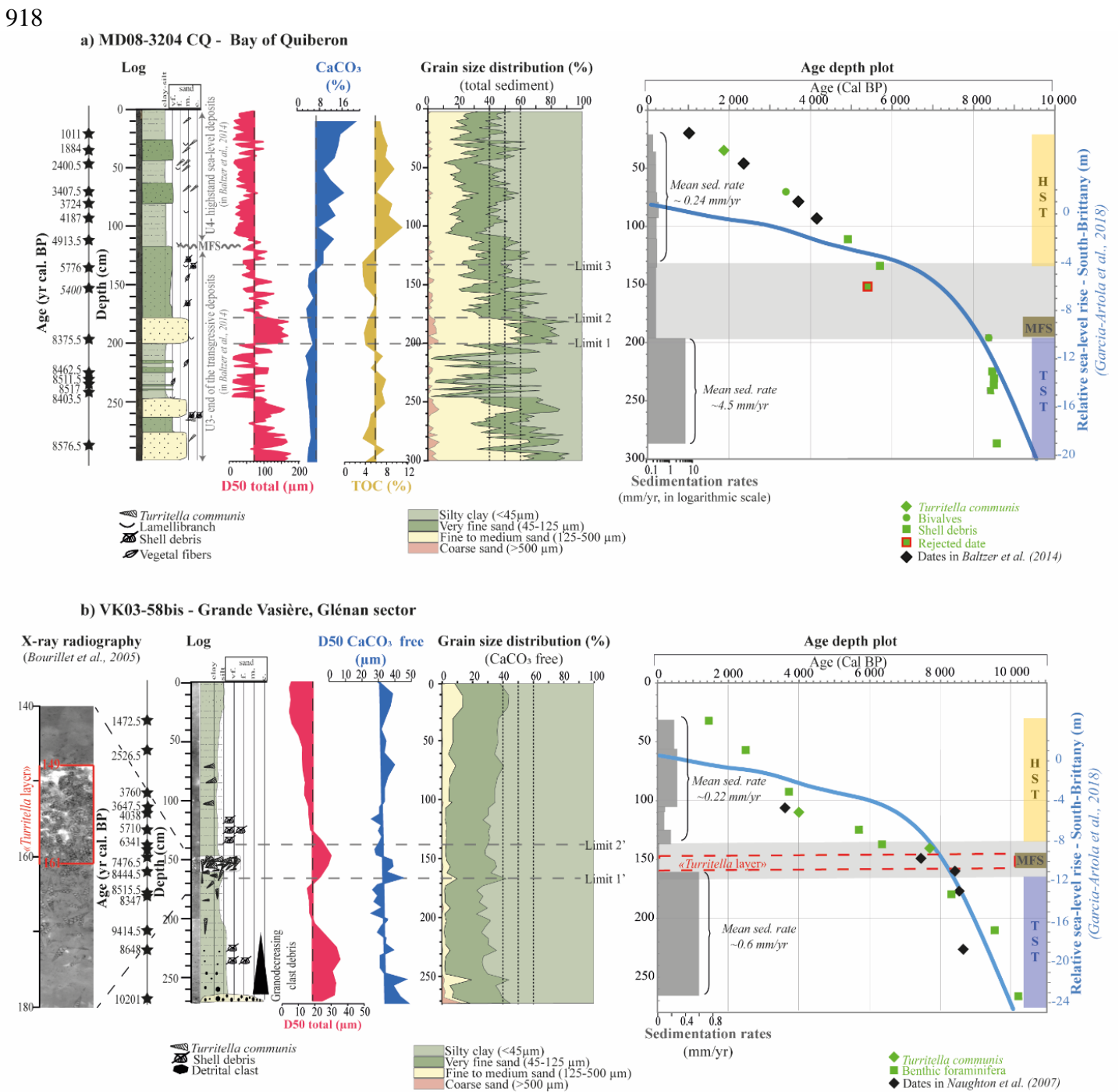
891 **Figure 1:** a) Map illustrating the general winter surface circulation in the Bay of Biscay  
 892 (*Koutsikopoulos and Le Cann, 1996; Ferrer et al., 2009*), the repartition of muddy deposits on  
 893 the shelf (*Allen and Castaing, 1977*), the location of the studied cores MD08-3204 CQ (Bay of  
 894 Quiberon; *Baltzer et al., 2014*; I on the map a) and VK03-58bis (northern Grande Vasière,  
 895 South Glénan islands; *Bourillet et al., 2005, 2006; Naughton et al., 2007*; II on the map a) as  
 896 well as other cited cores in the text, including GL3 (loc'h of Guidel; *Fernane et al., 2015*; 1 on  
 897 the map a), CBT-CS11 (northern Grande Vasière, Penmarc'h sector; *Mojtahid et al., 2019*;  
 898 *Penaud et al., 2020*; 2 on the map a), VC-08 (Bay of Douarnenez; *Lambert et al., 2019*; 3 on  
 899 the map a) and MD95-2002 (Meriadzec Terrace; *Zumaque et al., 2017; Fersi et al., in prep.*; 4  
 900 on the map a). b) Surface sediment distribution over the South Armorican platform (*Lesueur  
 901 and Klingebiel, 1986; Menier et al., 2014*) and location of the above mentioned inner to mid-  
 902 shelf cores.



903 **Figure 2:** a) Age model of the studied core MD08-3204 CQ over the last 5.7 kyrs BP. b)  
 904 Revised age models for cores CBT-CS11 (*Penaud et al., 2020*) and GL3 (*Fernane et al., 2015*).  
 905 Age models were established using the rbacon package (*Blaauw and Christen, 2011*) in R  
 906 version 4.1.2, and are expressed along cultural subdivisions for western Brittany (*Gorzynska*  
 907 *et al., in prep*) and stratigraphical subdivisions (*Walker et al., 2019*).

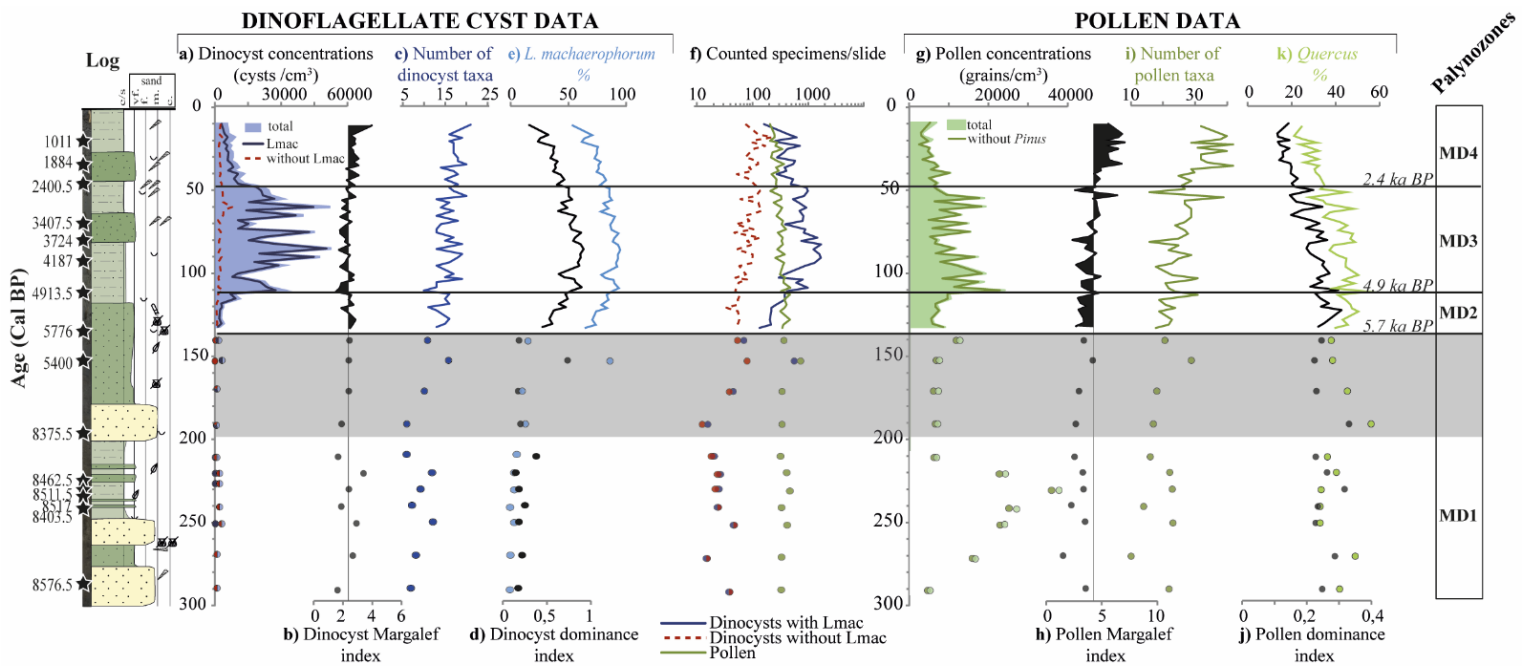


908 **Figure 3:** Sedimentological description for cores a) MD08-3204 CQ and b) VK03-58bis,  
 909 including the logs for the description of the sedimentary facies (a and b), X-ray radiography  
 910 (*Bourillet et al., 2005*; only b), the median grain-size analysis or D50 on total (a and b) and  
 911 decarbonated (only b) sediments, grain-size distributions (regarding total sediments for a and  
 912 decarbonated sediments for b), as well as Total Organic Carbon (TOC) measurements (only a).  
 913 Age-depth plots for both cores (see Tables 1 and 2) are represented along sedimentation rates  
 914 and the relative sea level (RSL) for southern Brittany (*García-Artola et al., 2018*). Intervals of  
 915 low sedimentation rates linked to sediment remobilization and/or non-deposits are indicated  
 916 using grey horizontal bands. HST: Highstand System Tract; TST: Transgressive System Tract;  
 917 MFS: Maximum Flooding Surface.

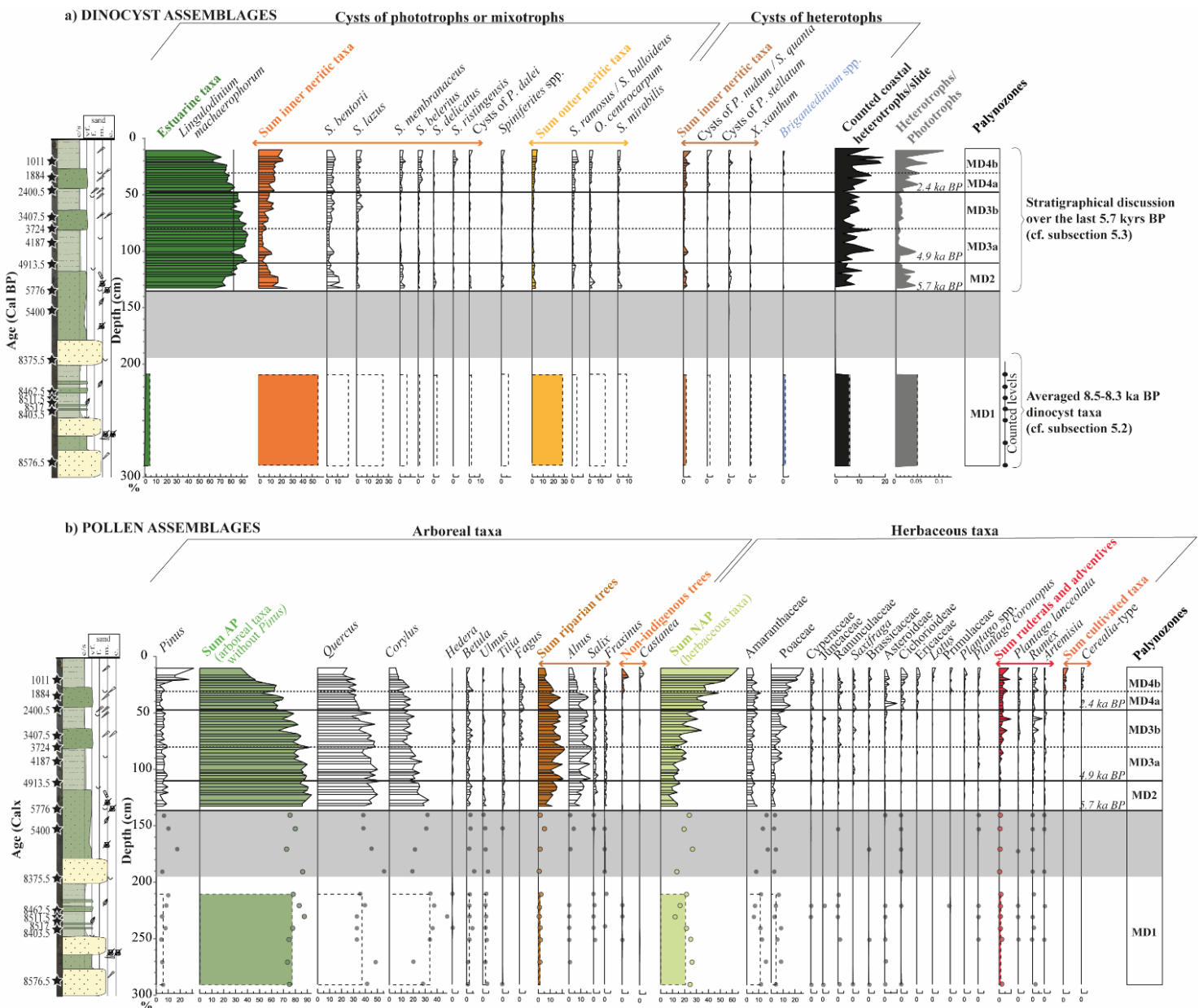


919 **Figure 4:** Along the log of core MD08-3204 CQ (see Fig. 3a): Palynological (dinocyst and  
 920 pollen) data plotted vs. depth (cm) with concentrations (a and g), diversity Margalef indexes (b  
 921 and h), number of different taxa (c and i), as well as dominance indexes (d and j) in parallel  
 922 with percentages of the dominant species in dinocyst and pollen assemblages (e and k,  
 923 respectively). Also, the number of counted specimens per analysed sample for pollen and  
 924 dinocysts is highlighted in logarithmic scale allowing better visualizing the few number of  
 925 dinocysts counted in the lower section of the MD08-3204CQ core. The interval of low  
 926 sedimentation rates linked to sediment remobilization and/or non-deposits is indicated using a  
 927 grey horizontal band (see Fig. 3a).

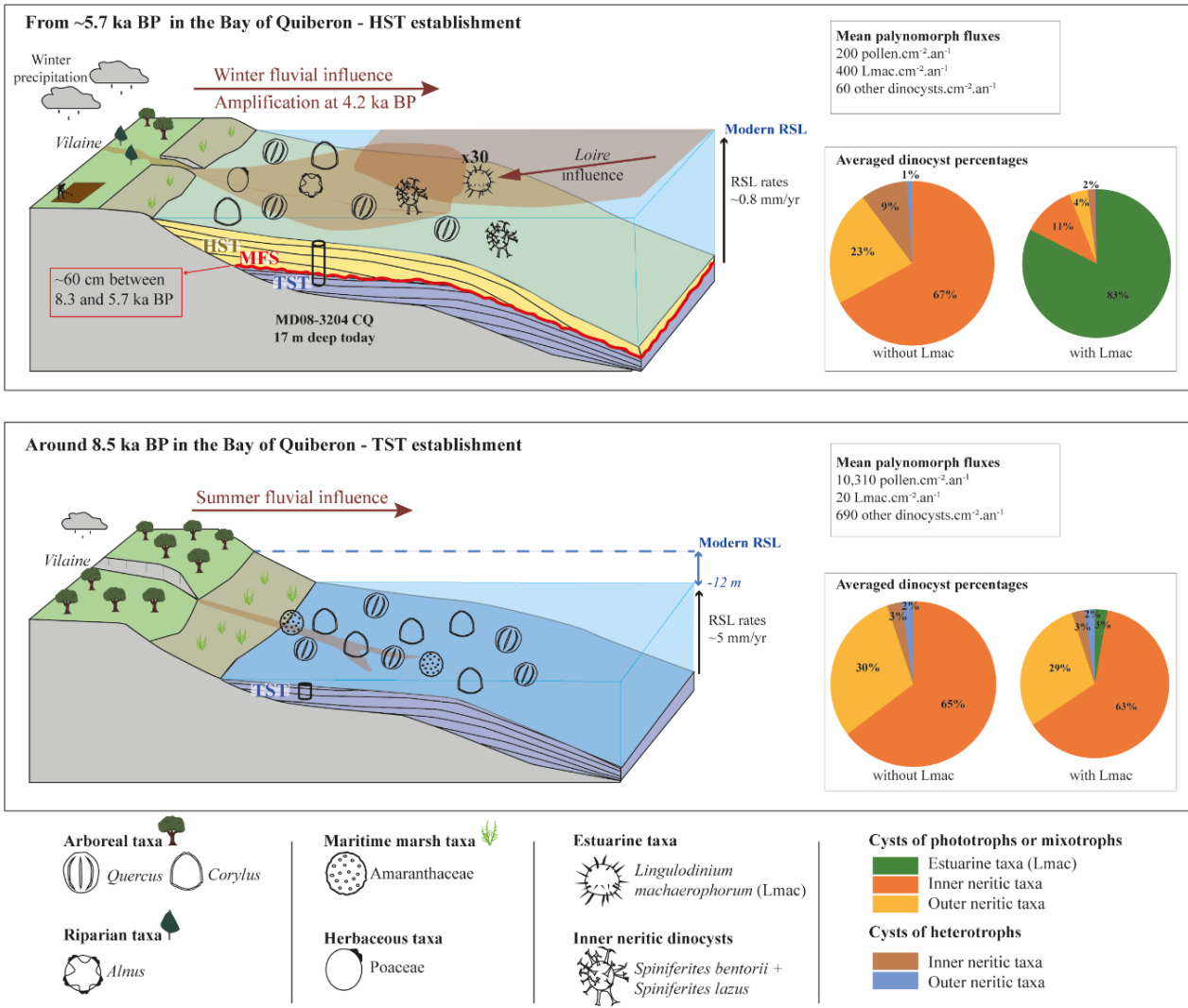
928



929 **Figure 5:** MD08-3204 CQ palynological data plotted vs. depth (cm). Major taxa (greater than  
 930 2% at least once in analyzed samples) of a) dinocyst and b) pollen assemblages. The interval of  
 931 low sedimentation rates linked to sediment remobilization and/or non-deposits is indicating  
 932 using grey horizontal bands (see Fig. 3a). Dinoflagellate cyst data are not represented for the  
 933 latter interval, and they have been summed between 290 and 210 cm due to the extremely low  
 934 dinocyst counts (see Fig 4). Regarding pollen data, points are represented in the grey band but  
 935 will never be considered in the discussion. An average of the basal points will be considered  
 936 for the discussion, as for dinocysts. Colored percentages highlight dinocyst and pollen groups  
 937 (see Table 3).  
 938

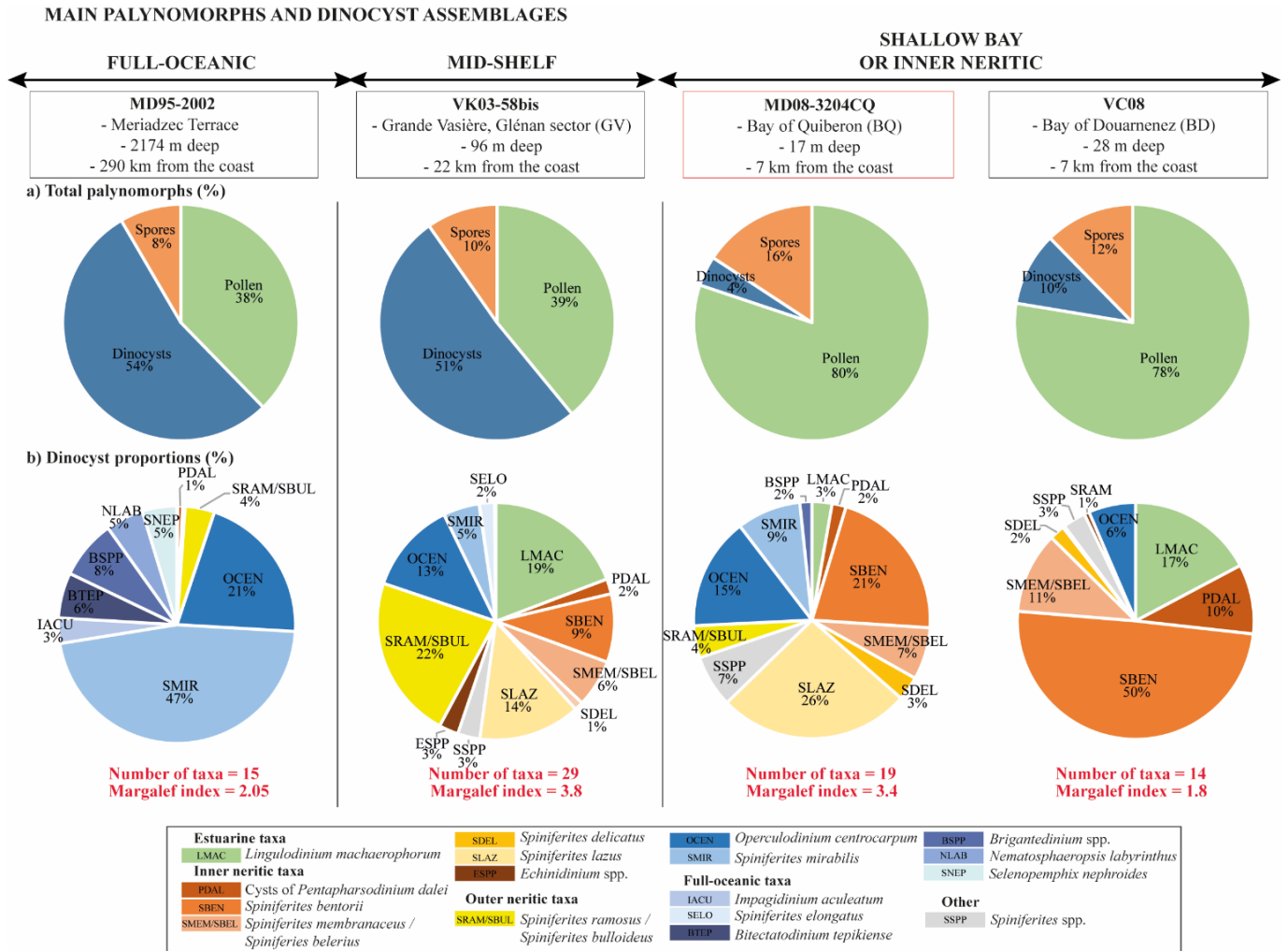


939 **Figure 6:** Conceptual model illustrating sedimentological configurations and main  
 940 palynological tracers recorded at around 8.5 ka BP and from ~5.7 ka BP in the Bay of Quiberon.  
 941 The number of palynomorphs represented in the two figures, respects the proportion of  
 942 specimens counted for the two intervals (i.e., 8.5-8.3 ka BP and 5.7-1 ka BP) and are based on  
 943 an arbitrary initial value of 4 grains of *Quercus* for the interval 5.7-1 ka BP. On both intervals  
 944 dinocyst group (see Table 3; Fig. 5) percentages were also averaged.

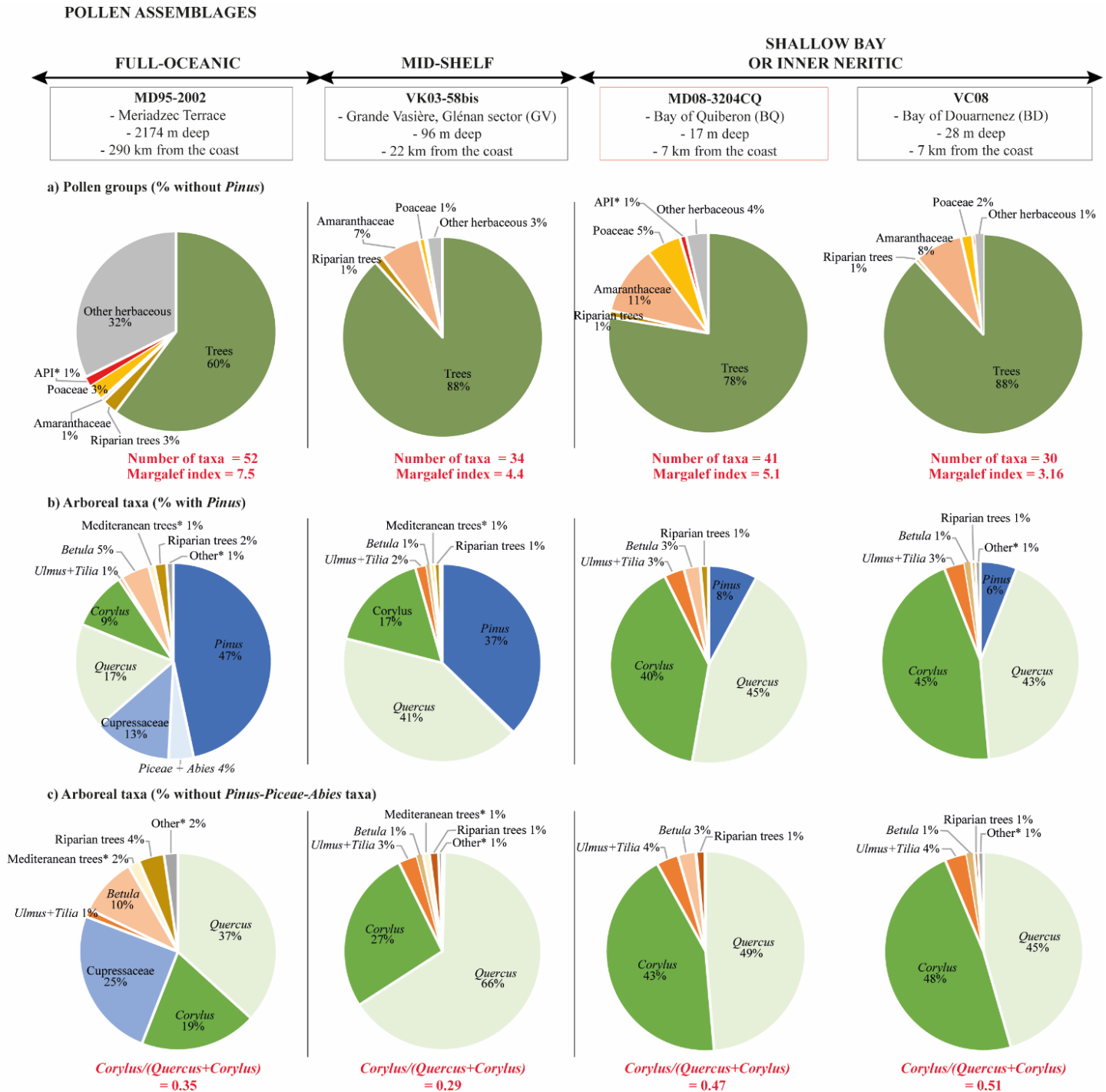




945 **Figure 7:** 8.5–8.3 ka BP averaged palynomorph (a) and dinocyst (b) data (~200 yrs) along an  
 946 inshore-offshore gradient with two proximal cores (MD08-3204 CQ, Bay of Quiberon, this  
 947 study; and VC-08, Bay of Douarnenez, *Lambert et al., 2019*) and two distal cores (VK03-58bis,  
 948 Grande Vasière, Glénan sector, *Naughton et al., 2007; Penaud, pers. comm.*; and MD95-2002,  
 949 Meriadzec Terrace, *Zumaque et al., 2017; Fersi, et al., in prep.*). See Fig. 1 for core locations.

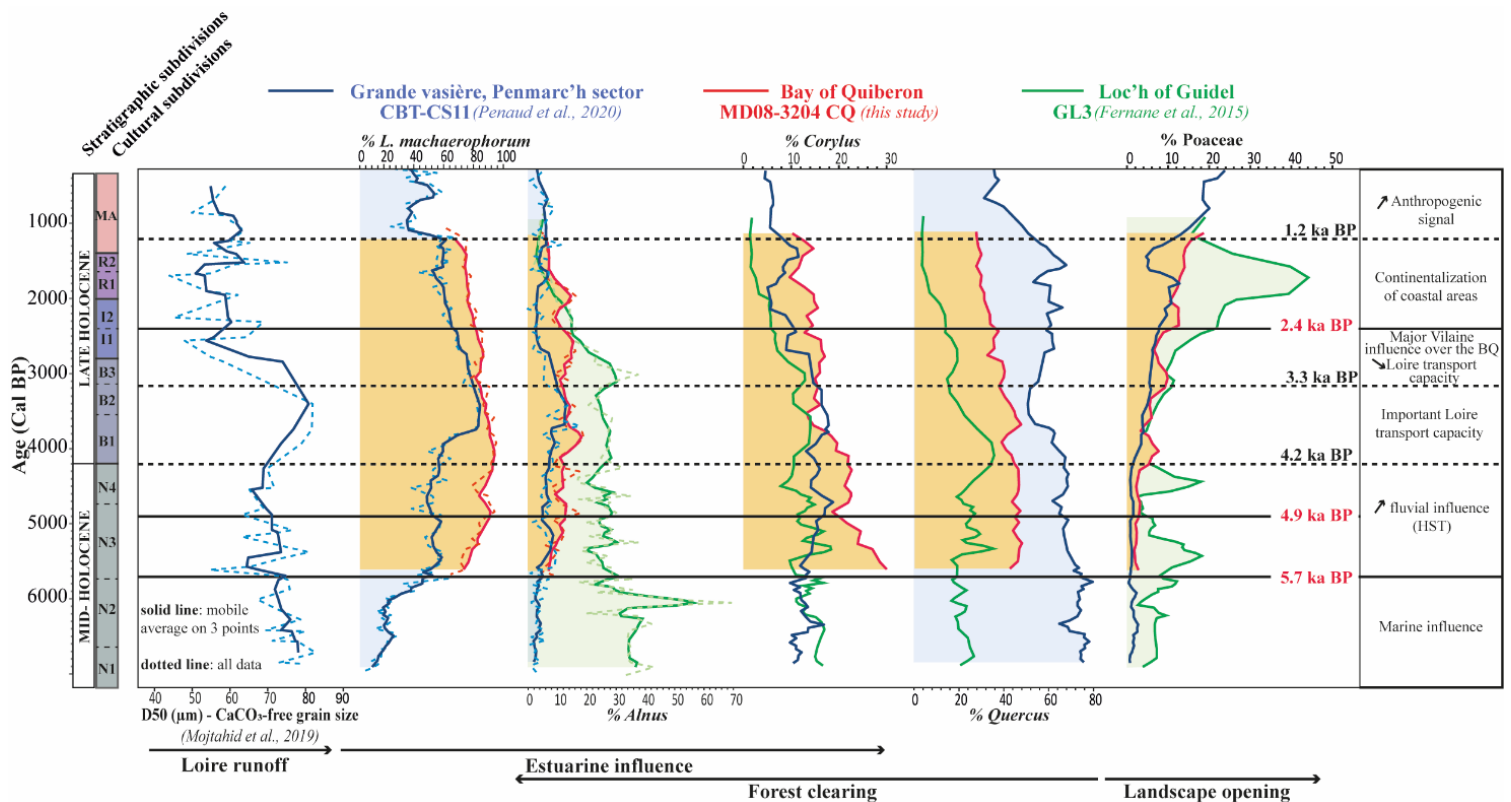


950 **Figure 8:** 8.5–8.3 ka BP averaged pollen data (~200 yrs) along an inshore-offshore gradient  
 951 with two proximal cores (MD08-3204 CQ, Bay of Quiberon, this study; and VC-08, Bay of  
 952 Douarnenez, *Lambert et al., 2019*) and two distal cores (VK03-58bis, Grande Vasière, Glénan  
 953 sector, *Naughton et al., 2007; Penaud, pers. comm.*; and MD95-2002, Meriadzec Terrace,  
 954 *Zumaque et al., 2017; Fersi, et al., in prep.*). See Fig. 1 for core locations.

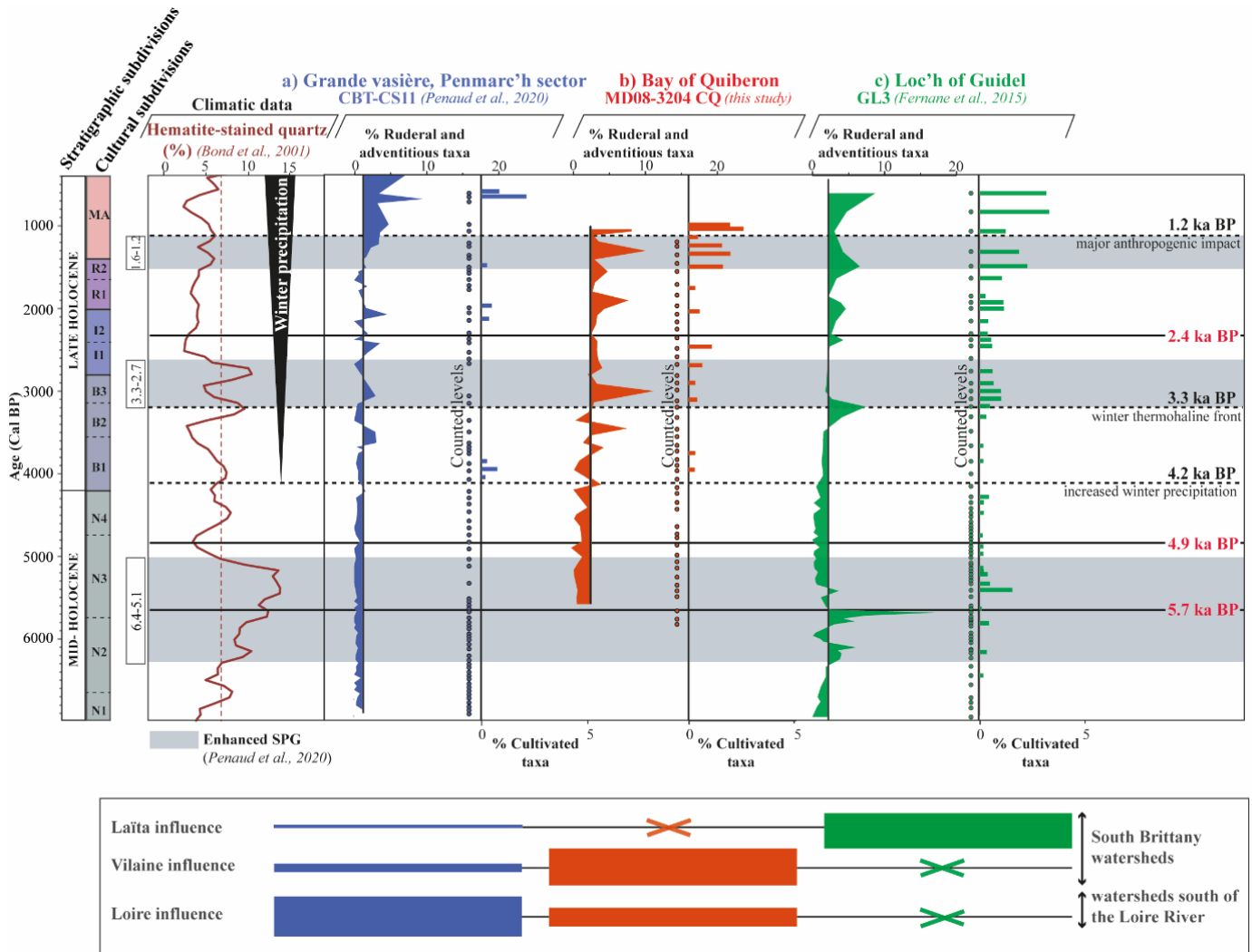


API\*: *Cannabaceae*, *Cerealia*-type, *Plantago lanceolata*, *Centaurea*, *Rumex* / **Mediterranean trees\***: *Quercus suber*, *Quercus ilex* / **Other\***: main sum taxa <2%

955 **Figure 9:** Selected palynological data (i.e., *Lingulodinium machaerophorum*, *Alnus*, *Quercus*,  
 956 *Corylus*, Poaceae) acquired on cores MD08-3204 CQ (in orange; this study), CBT-CS11 (in  
 957 blue; Penaud et al., 2020) and GL3 (in green; Fernane et al., 2015) addressed in parallel with  
 958 stratigraphical and cultural subdivisions (see Fig. 2). Note the additional sedimentological data  
 959 from core CBT-CS11 (i.e., D50 grain size on decarbonated sediments; Mojtahid et al., 2019)  
 960 in order to discuss the load-transport capacity of the Loire river. Straight horizontal lines  
 961 correspond to limits between MD08-3204 CQ palynozones. Dotted horizontal lines correspond  
 962 to hydrodynamic (4.2 and 3.3 ka BP) or anthropogenic (1.2 ka BP) thresholds previously  
 963 identified (Penaud et al., 2020).



964 **Figure 10:** Anthropogenic Pollen Indicators (API: ruderal and adventitious taxa, cultivated  
 965 taxa; see Table 3) calculated for cores MD08-3204 CQ (in orange; this study), CBT-CS11 (in  
 966 blue; *Penaud et al., 2020*), and GL3 (in green; *Fernane et al., 2015*). Palynological data are  
 967 addressed in parallel with periods of subpolar gyre (SPG) strengthening (cf. *Penaud et al.,*  
 968 *2020*), represented using grey horizontal bands. See Fig. 1 for core and rivers locations, as well  
 969 as Fig. 2 for cultural subdivisions. Straight horizontal lines correspond to limits between MD08-  
 970 3204 CQ palynozones. Dotted horizontal lines correspond to hydrodynamic (4.2 and 3.3 ka BP)  
 971 or anthropogenic (1.2 ka BP) thresholds previously identified (*Penaud et al., 2020*).



972 **11. References**

- 973 Allen, G.P., Castaing, P., 1977. Carte de répartition des sédiments superficiels sur le plateau continental  
974 du Golfe de Gascogne. Bull. Inst. Géol. Bassin d'Aquitaine, 21, 255–261.
- 975
- 976 Alley, R.B., Marotzke, J., Nordhaus, W.D., Overpeck, J.T., Peteet, D.M., Pielke, R.A., Pierrehumbert,  
977 R.T., Jr, Rhines, P.B., Stocker, T.F., Talley, L.D., Wallace, J.M. 2003. Abrupt climate change. Science,  
978 299, 2005–2010. doi/10.1126/science.1081056
- 979
- 980 Andreieff, P., Bouysse, P., Châteauneuf, J.-J., L'Homer, A., Scolari, G., 1971. La couverture  
981 sédimentaire meuble du plateau continental externe de la Bretagne méridionale (Nord du golfe de  
982 Gascogne). Cahiers Océanographiques, 23, 343–381.
- 983
- 984 Arthuis, R., Goubert, E., Nauleau, J.F., 2015. Essai de reconstitution paléogéographique de la Loire par  
985 l'étude de la documentation existante. In "L'environnement en mémoire: marqueurs, outils et  
986 perspectives, Bardot-Cambot & Tranoy (coord), Ed. Presses Universitaires de Rennes, 75–88.
- 987
- 988 Arthuis, R., 2020. Les changements hydromorphologiques de l'estuaire de la Loire et l'évolution du  
989 port de Rezé/Ratiatum (Loire-Atlantique). Gallia, 77-1, 55–66. <https://doi.org/10.4000/gallia.5317>
- 990
- 991 Ayache, M., Swingedouw, D., Mary, Y., Eynaud, F., Colin, C., 2018. Multi-centennial variability of the  
992 AMOC Over the Holocene: A New Reconstruction Based on Multiple Proxy-derived SST Records.  
993 Glob. Planet. Change 170, 172-189. <https://doi.org/10.1016/j.gloplacha.2018.08.016>
- 994
- 995 Baltzer, A., Walter-Simonnet, A.-V., Mokeddem, Z., Tessier, B., Goubert, E., Cassen, S., Diffo, A.,  
996 2014. Climatically-driven impacts on sedimentation processes in the Bay of Quiberon (south-Brittany,  
997 France) over the last 10,000 years. Holocene, 24, 679–688. <https://doi.org/10.1177/0959683614526933>
- 998
- 999 Baltzer, A., Mokeddem, Z., Goubert, E., Larteaud, F., Labourdette, N., Fournier, J., Bourillet, J.-F.,  
1000 2015. The "Turritella Layer": A Potential Proxy of a Drastic Holocene Environmental Change on the  
1001 North–East Atlantic Coast. In: Maanan M., Robin M. (eds) Sediment Fluxes in Coastal Areas. Coastal  
1002 Research Library, vol 10. Springer, Dordrecht. [https://doi.org/10.1007/978-94-017-9260-8\\_1](https://doi.org/10.1007/978-94-017-9260-8_1)
- 1003
- 1004 Bassinot, F.C, Labeyrie, L.D., 1996. IMAGES - MD 101 à bord du Marion-Dufresne du 29 mai au 11  
1005 juillet 1995. A coring cruise of the R/V Marion Dufresne in the North Atlantic Ocean and Norwegian  
1006 Sea. Les Publications de l'Institut français pour la recherche et la technologie polaires. Les Rapports des  
1007 campagnes à la mer, (96-1), 221p. <https://archimer.ifremer.fr/doc/00633/74461/>

1008  
1009 Barbier, D., 1999. Histoire de la végétation du nord-mayennais, de la fin du Weichsélien à l'aube du  
1010 XXIe siècle. Mise en évidence d'un Tardiglaciaire armoricain. Interactions homme/milieu, Groupe  
1011 d'Études des Milieux Naturels, t. 1, texte, 285 p., t. 2, illustrations, 62 p., Nantes.  
1012  
1013 Benito, G., Macklin, M.G., Zielhofer, C., Jones, A.F., Machado, M.J., 2015. Holocene flooding and  
1014 climate change in the Mediterranean. *Catena*, 130, 13-33. <https://doi.org/10.1016/j.catena.2014.11.014>  
1015  
1016 Bennet, K.D., 1992. Psimpoll- Quickbasic Program That Generates Postscript Page Description of  
1017 Pollen Diagrams. INQUA Commission for the Study of the Holocene: Working Group on Data-  
1018 Handling Methods, Newsletter 8, 11–12.  
1019  
1020 Bégeot, C., 1998. Le comportement pollinique du Noisetier (*Corylus avellana*), son rôle comme  
1021 indicateur d'impacts anthropiques ? L'exemple d'un transect dans le sud du Jura. *Acta bot. Gallica*, 145  
1022 (4), 271–277. <https://doi.org/10.1080/12538078.1998.10516307>  
1023  
1024 Berger, A., Loutre, M.F., 1991. Insolation values for the climate of the last 10 million years. *Quat. Sci.*  
1025 *Rev.* 10 (4), 297–317. [https://doi.org/10.1016/0277-3791\(91\)90033-Q](https://doi.org/10.1016/0277-3791(91)90033-Q)  
1026  
1027 Beug, H.-J., 1961. Beiträge Zur Postglazialen Floren- Und Vegetationsgeschichte in Süddalmatien: Der  
1028 See „Malo Jezero“ Auf Mljet: Teil I: Vegetationsentwicklung. *Flora Oder Allg. Bot. Ztg.* 150 (4), 600–  
1029 631. [https://doi.org/10.1016/S0367-1615\(17\)33232-9](https://doi.org/10.1016/S0367-1615(17)33232-9)  
1030  
1031 Blaauw, M., Christen, J.A., 2011. Flexible paleoclimate age-depth models using an autoregressive  
1032 gamma process. *Bayesian Anal.* 6 (3), 457–474. DOI: 10.1214/11-BA618  
1033  
1034 Blamart D., Baltzer, A., Volker, A., 2008. MD 169 / MICROSYSTEMS cruise, RV Marion Dufresne,  
1035 <https://doi.org/10.17600/8200100>.  
1036  
1037 Blott, S.J. and Pye, K., 2001. GRADISTAT: a grain size distribution and statistics package for the  
1038 analysis of unconsolidated sediments. *Earth Surface Processes and Landforms*, 26, 1237–1248.  
1039 <https://doi.org/10.1002/esp.261>  
1040  
1041 Bond, G., Showers, W., Cheseby, M., Lotti, R., Almasi, P., deMenocal, P., Priore, P., Cullen, H., Hajdas,  
1042 I., Bonani, G., 1997. A pervasive millennial-scale cycle in North Atlantic Holocene and glacial climates.  
1043 *Science*, 278, 1257–1266. <https://doi.org/10.1126/science.278.5341.1257>  
1044

1045 Bond, G., Kromer, B., Beer, J., Muscheler, R., Evans, M., Showers, W., Hoffmann, S., LottiBond, R.,  
1046 Hajdas, I., Bonani, G. 2001. Persistent solar influence on North Atlantic climate during the Holocene.  
1047 Science, 294, 2130–36. <https://doi.org/10.1126/science.1065680>  
1048

1049 Bourillet, J-F., Dubrulle, C., Goubert, E., Jouanneau, J-M., Cortij, E., Weber, O., Lesueur, P., 2005. La  
1050 Grande Vasière : architecture, mise en place et estimation des facteurs de son évolution. Colloque Golfe  
1051 de Gascogne. 22-24 mars 2005, Brest. <https://archimer.ifremer.fr/doc/00749/86127/>  
1052

1053 Bourillet, J-F., Jouanneau, J-M., Macher, C., Le Hir, P., Naughton, F., 2006. “La Grande Vasière” mid-  
1054 shelf mud belt: Holocene sedimentary structure, natural and anthropogenic impact. In Abstracts of the  
1055 X International Symposium on Oceanography of the Bay of Biscay. Vigo, Spain, 19-21 April 2006,  
1056 131–134. <https://archimer.ifremer.fr/doc/00000/6243/>  
1057

1058 Broström, A., Nielsen, A.B., Gaillard, M.-J., Hjelle, K., Mazier, F., Binney, H., Bunting, J., Fyfe, R.,  
1059 Meltsov, V., Poska, A., 2008. Pollen productivity estimates of key European plant taxa for quantitative  
1060 reconstruction of past vegetation: a review. Veg. Hist. Archaeobotany, 17, 461–478.  
1061 <https://doi.org/10.1007/s00334-008-0148-8>  
1062

1063 Carter, M.C., 2008. *Turritella communis* An auger shell. In Tyler-Walters H. and Hiscock K. (eds)  
1064 Marine Life Information Network : Biology and Sensitivity Key Information Reviews, [on-line].  
1065 Plymouth: Marine Biological Association of the United Kingdom.  
1066

1067 Castaing, P., Allen, G.P., 1981. Mechanisms controlling seaward escape of suspended sediment from  
1068 the Gironde: A macrotidal estuary in France. Mar. Geol. 40(1), 101–118. [https://doi.org/10.1016/0025-3227\(81\)90045-1](https://doi.org/10.1016/0025-3227(81)90045-1)  
1069  
1070

1071 Castaing, P., Froidefond, J.M., Lazure, P., Weber, O., Prud’homme, R., Jouanneau, J.M., 1999.  
1072 Relationship between hydrology and seasonal distribution of suspended sediments on the continental  
1073 shelf of the Bay of Biscay. Deep Sea Research Part II: Topical Studies in Oceanography 46(10), 1979-  
1074 2001. [https://doi.org/10.1016/S0967-0645\(99\)00052-1](https://doi.org/10.1016/S0967-0645(99)00052-1)  
1075

1076 Castanet C., 2008. La Loire en val d’Orléans. Dynamiques fluviales et socio-environnementales durant  
1077 les derniers 30 000 ans : de l’hydrosystème à l’anthroposystème, Thèse de doctorat, Université de Paris-  
1078 1 Panthéon-Sorbonne, 549 p.  
1079

1080 Charria, G., Lazure, P., Le Cann, B., Serpette, A., Reverdin, G., Louazel, S., Batifoulier, F., Dumas, F.,

1081 Pichon, A., Morel, Y., 2013. Surface layer circulation derived from Lagrangian drifters in the Bay of  
1082 Biscay. *J. Mar. Syst.*, S60-S76. DOI: 10.1016/j.jmarsys.2011.09.015  
1083  
1084 Charria, G., 2018. Evolutions interannuelles de la circulation dans le golfe de Gascogne - vers une  
1085 dynamique à (sous)mésoéchelle en milieu côtier. Observer et simuler un océan côtier turbulent. HDR.  
1086 <https://archimer.ifremer.fr/doc/00475/58702/>  
1087  
1088 Chaumillon, E., Proust, J.-N., Menier, D., Weber, N., 2008. Incised-valley morphologies and  
1089 sedimentary-fills within the inner shelf of the Bay of Biscay (France): a synthesis. *J. Mar. Syst.*, 72, 383-  
1090 396. <https://doi.org/10.1016/j.jmarsys.2007.05.014>  
1091  
1092 Costoya, X., Fernandez-Novoa, D., deCastro, M., Santos, F., Lazure, P., Gomez-Gesteira, M., 2016.  
1093 Modulation of sea surface temperature warming in the Bay of Biscay by Loire et Gironde Rivers. *J.*  
1094 *Geophys. Res. Oceans*, 120, 14 p. <https://doi.org/10.1002/2015JC011157>  
1095  
1096 Cyprien, A.L., 2002. Chronologie de l'interaction de l'homme et du milieu dans l'espace central et aval  
1097 de la Loire (Ouest de la France). Thèse doctorat, Université de Nantes, Tome I, 183 pp ; Tome II, 75 pp.  
1098  
1099 Delaine, M., Châtelet, E., Bout-Roumazelles, V., Goubert, E., Le Cadre, E., Recourt, P., Trentesaux,  
1100 A., Arthuis, R., 2015. Multiproxy approach for Holocene paleoenvironmental reconstructions from  
1101 microorganisms (testate amoebae and foraminifera) and sediment analyses: The infilling of the Loire  
1102 Valley in Nantes (France). *Holocene* 25, 407–420. <https://doi.org/10.1177/0959683614561883>  
1103  
1104 de Vernal, A., Henry, M., Bilodeau, G., 1999. Technique de préparation et d'analyse en  
1105 micropaléontologie. Les Cahiers du GEOTOP vol. 3, Université du Québec à Montréal, Montréal,  
1106 Canada.  
1107  
1108 de Vernal, A., Radi, T., Zaragosi, S., Van Nieuwenhove, N., Rochon, A., Allan, E., De Schepper, S.,  
1109 Eunaud, F., Head, M.J., Limoges, A., Londeix, S., Marret, F., Matthiessen, J., Penaud, A., Pospelova,  
1110 V., Price, A., Richerol, T., 2020. Distribution of common modern dinoflagellate cyst taxa in surface  
1111 sediments of the Northern Hemisphere in relation to environmental parameters: The new n= 1968  
1112 database. *Mar. Micropaleontol.*, 159, 101796. <https://doi.org/10.1016/j.marmicro.2019.101796>  
1113  
1114 Dubrulle, C., Jouanneau, J.M., Lesueur, P., Bourillet, J.F., Weber, O., 2007. Nature and rates of fine-  
1115 sedimentation on a mid-shelf: “La Grande Vasière” (Bay of Biscay, France). *Cont. Shelf Res.* 27, 2099-  
1116 2115. <https://doi.org/10.1016/j.csr.2007.05.002>  
1117



1118 Dussud, L., 2010. CABTEX cruise, RV Pourquoi pas ? <https://doi.org/10.17600/10030050>.  
1119  
1120 Engelhart, S.E., Horton, B.P., 2012. Holocene sea level database for the Atlantic coast of the United  
1121 State. *Quat. Sci. Rev.* 54, 12–25. <https://doi.org/10.1016/j.quascirev.2011.09.013>  
1122  
1123 Fatela, F., Taborda, R., 2002. Confidence limits of species proportions in microfossil assemblages. *Mar.*  
1124 *Micropaleontol.* 45, 169–174. [https://doi.org/10.1016/S0377-8398\(02\)00021-X](https://doi.org/10.1016/S0377-8398(02)00021-X)  
1125  
1126 Fernane, A., Gandouin, E., Penaud, A., Van Vliet-Lanoë, B., Goslin, J., Vidal, M., Delacourt, C., 2014.  
1127 Coastal palaeoenvironmental record of the last 7 ka BP in NW France: sub-millenary climatic and  
1128 anthropic Holocene signals. *Holocene* 24, 1785–1797. <https://doi.org/10.1177%2F0959683614551223>  
1129  
1130 Fernane, A., Penaud, A., Gandouin, E., Goslin, J., Van Vliet-Lanoë, B., Vidal, M., 2015. Climate  
1131 variability and storm impacts as major drivers for human coastal marsh withdrawal over the Neolithic  
1132 period (Southern Brittany, NW France). *Palaeogeogr., Palaeoclimatol., Palaeoecol.* 435, 136–144.  
1133 <https://doi.org/10.1016/j.palaeo.2015.05.029>  
1134  
1135 Ferrer, L., Fontán, A., Mader, J., Chust, G., González, M., Valencia, V., Uriarte, Ad., Collins, M. B.,  
1136 2009. Low-salinity plumes in the oceanic region of the Basque Country. *Continental Shelf Research*,  
1137 29, 8, 970–984. DOI: 10.1016/j.csr.2008.12.014.  
1138  
1139 Fersi, W., Penaud, A., David, O., Lambert, C., Vidal, M., Stéphan, P., Zumaque, J., De Vernal, A.,  
1140 Eynaud, F., in prep. Paleoenvironmental signature of Holocene records from the northern margin of the  
1141 Bay of Biscay.  
1142  
1143 Folliot, B., 2004. La Grande Vasière : Etude sédimentologique de deux secteurs septentrionaux. Rapport  
1144 de DEA Dynamique et Environnements Sédimentaires, Université Lille-Caen-Rouen, p.39.  
1145  
1146 Fujiwara, O., Kamataki, T., Masuda, F., 2004. Sedimentological time-averaging and <sup>14</sup>C dating of  
1147 marine shells. *Nucl. Instrum. Methods Phys. Res., B Beam Interact. Mater. Atoms* 223–224, 540–544.  
1148 <https://doi.org/10.1016/j.nimb.2004.04.101>  
1149  
1150 Funder, S., Demidov, I., Yelovicheva, Y., 2002. Hydrography and mollusc faunas of the Baltic and the  
1151 White Sea–North Sea seaway in the Eemian. *Palaeogeogr., Palaeoclimatol., Palaeoecol.* 184, 275–304.  
1152 [http://dx.doi.org/10.1016/S0031-0182\(02\)00256-0](http://dx.doi.org/10.1016/S0031-0182(02)00256-0)  
1153

1154 Ganne, A., Leroyer, C., Penaud, A., Mojtahid, M., 2016. Present-day palynomorph deposits in an  
1155 estuarine context: the case of the Loire Estuary. *J. Sea Res.* 118, 35–51.  
1156 <https://doi.org/10.1016/j.seares.2016.10.006>  
1157  
1158 García-Artola, A., Stéphan, P., Cearreta, A., Kopp, R.E., Khan, N.S., Horton, B.P., 2018. Holocene sea-  
1159 level database from the Atlantic coast of Europe. *Quat. Sci. Rev.* 196, 177–192.  
1160 <https://doi.org/10.1016/j.quascirev.2018.07.031>  
1161  
1162 García-Mozo, H., Galán, C., Jato, V., Belmonte, J., 2006. *Quercus* pollen season dynamics in the Iberian  
1163 peninsula: response to meteorological parameters and possible consequences of climate change. *Ann.*  
1164 *Agric. Environ. Med.* 13, 209–224.  
1165  
1166 Gaudin, L., 2004. Transformations spatio-temporelles de la végétation du nord-ouest de la France depuis  
1167 la fin de la dernière glaciation. Reconstitutions paléo-paysagères. Thèse doctorat, Université de Rennes  
1168 I, 660 pp. <https://tel.archives-ouvertes.fr/tel-00470150>  
1169  
1170 Giraudeau, J., Grelaud, M., Solignac, S., Andrews, J., Moros, M., Jansen, E., 2010. Millennial scale  
1171 variability in Atlantic water advection to the Nordic seas derived from Holocene coccolith concentration  
1172 records. *Quat. Sci. Rev.* 29, 1276–1287. <https://doi.org/10.1016/j.quascirev.2010.02.014>  
1173  
1174 Goslin, J., Van Vliet Lanoë, B., Spada, G., Bradley, S., Tarasov, L., Neil, S. and Suanez, S., 2015. A  
1175 new Holocene relative sea-level curve for western Brittany (France): Insights on Isostatic dynamics  
1176 along the Atlantic coasts of north-western Europe. *Quat. Sci. Rev.* 129, 341–365.  
1177 <https://doi.org/10.1016/j.quascirev.2015.10.029>  
1178  
1179 Goslin, J., Fruergaard, M., Sander, L., Gałka, M., Menviel, L., Monkenbusch, J., Thibault, N.,  
1180 Clemmensen, L.B., 2018. Holocene centennial to millennial shifts in North-Atlantic storminess and  
1181 ocean dynamics. *Sci. Rep.* 8, 12778. <https://doi.org/10.1016/j.quascirev.2015.10.029>  
1182  
1183 Gorczynska, A., Stéphan, P., Pailler, Y., Nicolas, C., Penaud, A., David, O., Vidal, M., Le Gall, B.,  
1184 submitted, in prep. Holocene evolution of coastal dunes in western France: regional reconstruction from  
1185 archaeological and historical data. *Aeolian Research*.  
1186  
1187 Gregoire, G., Le Roy, P., Ehrhold, A., Jouet, G., and Garlan, T. 2017. Control factors of Holocene  
1188 sedimentary infilling in a semi-closed tidal estuarine-like system: the bay of Brest (France). *Mar. Geol.*  
1189 385, 84–100. <https://doi.org/10.1016/j.margeo.2016.11.005>  
1190

1191 Guilcher, A., 1948. Le relief de la Bretagne méridionale de la baie de Douarnenez à la Vilaine. PhD  
1192 Thesis, Paris, H. Potier (Ed.), La Roche-sur-Yvon. 682 p.  
1193

1194 Guillaud, J., Aminot, A., Delmas, D., Gohin, F., Lunven, M., Labry, C., Herbland, A., 2008. Seasonal  
1195 variation of riverine nutrient inputs in the northern Bay of Biscay (France), and patterns of marine  
1196 phytoplankton response. *J. Mar. Syst.* 72, 309–319. <https://doi.org/10.1016/j.jmarsys.2007.03.010>  
1197

1198 Hammer, Ø., Harper, D.A.T., Paul, D.R., 2001. Past: Paleontological Statistics Software Package for  
1199 Education and Data Analysis. *Paleontologia Electronica*, 4, 1, 9 p.  
1200

1201 Hátún, H., Sandø, A. B., Drange, H., Hansen, B., Valdimarsson, H., 2005. Influence of the Atlantic  
1202 subpolar gyre on the thermohaline circulation. *Science* 309, 1841–1844. DOI: 10.1126/science.1114777  
1203

1204 Heiri, O., Lotter, A.F., Lemcke, G., 2001. Loss on ignition as a method for estimating organic and  
1205 carbonate content in sediments: reproducibility and comparability of results. *Journal of paleolimnology*,  
1206 25, 101–110. <https://doi-org.scd-proxy.univ-brest.fr/10.1023/A:1008119611481>  
1207

1208 Holmes, P., 1994. The sorting of spores and pollen by water: experimental and field evidence. In:  
1209 Traverse, A. (Ed.), *Sedimentation of Organic Particles*. Cambridge University Press, Cambridge, 9–32.  
1210

1211 Hurrell, JW, 1995. Decadal trends in the North Atlantic Oscillation: regional temperatures and  
1212 precipitation. *Science* 269, 676–679. DOI: 10.1126/science.269.5224.676  
1213

1214 Hurrell, J.W., Kushnir, Y., Ottersen, G., Visbeck, M., 2003. The North Atlantic Oscillation: climate  
1215 significance and environmental impacts. *Geophys. Monogr. Ser.* 134, 279.  
1216

1217 Joly, C., Visset, L., 2009. Evolution of vegetation landscapes since the Late Mesolithic on the French  
1218 West Atlantic coast. *Rev. Palaeobot. Palynol.* 154, 124–179..  
1219 <https://doi.org/10.1016/j.revpalbo.2008.12.011>  
1220

1221 Jouanneau, J.-M., Weber, O., Cremer, M., Castaing, P., 1999. Fine-grained sediment budget on the  
1222 continental margin of the Bay of Biscay. *Deep-Sea Res., II*, 46, 2205–2220.  
1223 [https://doi.org/10.1016/S0967-0645\(99\)00060-0](https://doi.org/10.1016/S0967-0645(99)00060-0)  
1224

1225 Jouet, G., Augris, C., Hallegouët, B., Le Roy, P., Rolet, J., 2003. La vallée d'Ys: un paléoréseau  
1226 hydrographique immergé en baie de Douarnenez (Finistère, France). *Compt. Rendus Geosci.* 335 (5),  
1227 487–494. [https://doi.org/10.1016/S1631-0713\(03\)00066-X](https://doi.org/10.1016/S1631-0713(03)00066-X)

1228  
1229 Kidwell, S.M., 1997. Time-Averaging in the Marine Fossilrecord: Overview of Strategies and  
1230 Uncertainties. *Geobios*, 30 (7), 977–995. [https://doi.org/10.1016/S0016-6995\(97\)80219-7](https://doi.org/10.1016/S0016-6995(97)80219-7)  
1231  
1232 Koutsikopoulos, C., Le Cann, B., 1996. Physical processes and hydrological structures related to the  
1233 Bay of Biscay anchovy. *Sci. Mar.* 60, 9–19.  
1234  
1235 Lambert, C., Vidal, M., Penaud, A., Combourieu-Nebout, N., Lebreton, V., Ragueneau, O., Gregoire,  
1236 G., 2017. Modern palynological record in the Bay of Brest (NW France): Signal calibration for palaeo-  
1237 reconstructions. *Rev. Palaeobot. Palynol.* 244, 13–25. <https://doi.org/10.1016/j.revpalbo.2017.04.005>  
1238  
1239 Lambert, C., Penaud, A., Vidal, M., Klouch, K., Grégoire, G., Ehrold, A., Eynaud, F., Schmidt, S.,  
1240 Ragueneau, O., Sianno, R., 2018. Human-induced river runoff overlapping natural climate variability  
1241 over the last 150 years: palynological evidence (Bay of Brest, NW France). *Glob. Planet. Chang.* 160,  
1242 109–122. <https://doi.org/10.1016/j.gloplacha.2017.11.004>  
1243  
1244 Lambert C., Vidal M., Penaud A., Le Roy P., Goubert E., Pailler Y., Stéphan P., Ehrhold A., 2019.  
1245 Palaeoenvironmental reconstructions during the Meso- to Neolithic transition (9.2 – 5.3 cal ka BP) in  
1246 Northwestern France: palynological evidences. *Holocene* 29, 380–402.  
1247 <https://doi.org/10.1177%2F0959683618816457>  
1248  
1249 Lambert, C., Penaud, A., Vidal, M., Gandini, C., Labeyrie, L., Chauvaud, L., Ehrold, A., 2020. Striking  
1250 forest revival at the end of the Roman Period in north-western Europe. *Sci Rep* 10, 21984.  
1251 <https://doi.org/10.1038/s41598-020-77253-1>  
1252  
1253 Lambert, C., Penaud, A., Poirier, C., Goubert, E., 2022. Distribution of modern dinocysts in surface  
1254 sediments of southern Brittany (NW France) in relation to environmental parameters: Implications for  
1255 paleoreconstructions. *Rev. of Palaeobot. and Palynol.*, 297, 104578.  
1256 <https://doi.org/10.1016/j.revpalbo.2021.104578>  
1257  
1258 Lazure, P., Jégou, A.M., 1998. 3D modelling of seasonal evolution of Loire and Gironde plumes on  
1259 Biscay Bay continental shelf. *Oceanol. Acta.* 21, 165–177. [https://doi.org/10.1016/S0399-](https://doi.org/10.1016/S0399-1784(98)80006-6)  
1260 [1784\(98\)80006-6](https://doi.org/10.1016/S0399-1784(98)80006-6)  
1261  
1262 Lazure, P., Dumas, F., Vrignaud, C., 2008. Circulation on the Armorican shelf (Bay of Biscay) in  
1263 autumn. *J. Mar. Syst.* 72, 218–237. <https://doi.org/10.1016/j.jmarsys.2007.09.011>  
1264

1265 Lebreton, V., Messager, E., Marquer, L., Renault-Miskovsky, J., 2010. A neotaphonomic experiment in  
1266 pollen oxidation and its implications for archaeopalynology. *Rev. Palaeobot. Palynol.*, 162, 29–38.  
1267 <https://doi.org/10.1016/j.revpalbo.2010.05.002>  
1268  
1269 Leorri, E., Cearreta, A., Milne, G., 2012a. Field observations and modelling of Holocene sea-level  
1270 changes in the southern Bay of Biscay: implication for understanding current rates of relative sea-level  
1271 change and vertical land motion along the Atlantic coast of SW Europe. *Quat. Sci. Rev.* 42, 59–73.  
1272 <https://doi.org/10.1016/j.quascirev.2012.03.014>  
1273  
1274 Leorri, E., Fatela, F., Drago, T., Bradley, S.L., Moreno, J., Cearreta, A., 2012b. Lateglacial and  
1275 Holocene coastal evolution in the Minho estuary (N Portugal): implications for understanding sea-level  
1276 changes in Atlantic Iberia. *Holocene* 23, 353–363. <https://doi.org/10.1177/0959683612460786>  
1277  
1278 Le Roy, P., 2003. VIBARMOR cruise, RV Côtes De La Manche, <https://doi.org/10.17600/3480160>  
1279  
1280 Le Roy, P., Jouet, G., 2005. Remplissage sédimentaire meuble. In : Augris, C., Ménesguen, A., Hamon,  
1281 D., Blanchet, A., Le Roy, P., Rolet, J., Jouet, G., Véron, G., Delannoy, H., 1081 Drogou, M., Bernard,  
1282 C., Maillard, X., 2005. Atlas thématique de l'environnement marin de la Baie de Douarnenez. Ifremer  
1283 (Ed), 61–72.  
1284  
1285 Lesueur, P., Klingebiel, A., 1986. Carte des sédiments superficiels du plateau continental du Golfe de  
1286 Gascogne - Partie septentrionale au 1/500.000. Co-édition BRGM-Ifremer, carte géologique de la marge  
1287 continentale française, 1carte, 1 notice, 23 p.  
1288  
1289 Lesueur, P., Jouanneau, J.-M., Boust, D., Tastet, J.P., Weber, O., 2001. Sedimentation rates and fluxes  
1290 in the continental shelf mud fields in the Bay of Biscay (France). *Cont. Shelf Res.* 21, 1383–1401.  
1291 [https://doi.org/10.1016/S0278-4343\(01\)00004-8](https://doi.org/10.1016/S0278-4343(01)00004-8)  
1292  
1293 Lohmann, K., Drange, H., Bentsen, M., 2009. Response of the North Atlantic subpolar gyre to persistent  
1294 North Atlantic oscillation like forcing. *Clim. Dyn.* 32, 273–285. [https://doi.org/10.1007/s00382-008-](https://doi.org/10.1007/s00382-008-0467-6)  
1295 [0467-6](https://doi.org/10.1007/s00382-008-0467-6)  
1296  
1297 Marguerie, D., 1990. L'environnement à l'Age du Fer en Armorique. In: Duval A, Le Bihan JP and  
1298 Menez Y (eds) *Les Gaulois d'Armorique: actes du 12e colloque de l'AFEAF, Quimper 1988 (Suppl*  
1299 *Revue Archéologique de l'Ouest 3)*. Paris: Association Française pour l'Etude de 'l'Age du Fer, 115–  
1300 120.  
1301

1302 Marguerie, D., 1992. Évolution de la végétation sous l'impact humain en Armorique du Néolithique aux  
1303 périodes historiques. Rennes, Travaux du Laboratoire d'Anthropologie de l'Université de Rennes 1, n°  
1304 40, 313 p.  
1305  
1306 Marguerie, D., 1993. Histoire de la végétation armoricaine. L'apport des restes végétaux des sites  
1307 archéologiques et des tourbières. Penn ar Bed (Brest) 148-149, 32-45.  
1308  
1309 Marguerie, D., 2003. Bocages armoricains et sociétés, genèse, évolution et interactions. In: Des milieux  
1310 et des hommes: fragments d'histoires croisés. Paris, Elsevier, 115-131.  
1311  
1312 Marret, F., Bradley, L., de Vernal, A., Hardy, W., Kim, S. Y., Mudie, P., Penaud, A., Pospelova, V.,  
1313 Price, A., Radi, T., Rochon, A., 2020. From bi-polar to regional distribution of modern dinoflagellate  
1314 cysts, an overview of their biogeography. *Mar. Micropaleontol.*, 159, 101753.  
1315 <https://doi.org/10.1016/j.marmicro.2019.101753>  
1316  
1317 Mayewski, P.A., Rohling, E.E., Curt Stager, J., Karlén, W., Maasch, K.A., David Meeker, L., Meyerson,  
1318 E.A., Gasse, F., Van Kreveland, S., Holmgren, K., Lee-Thorp, J., Rosqvist, G., Rack, F., Staubwasse, M.,  
1319 Schneider, R.R., Steig, E.J., 2004. Holocene climate variability. *Quat. Res.* 62, 243-255.  
1320 <https://doi.org/10.1016/j.yqres.2004.07.001>  
1321  
1322 Mazier, F., Broström, A., Gaillard, M.-J., Sugita, S., Vittoz, P., and Buttier, A., 2008. Pollen productivity  
1323 estimates and relevant source area of pollen for selected plant taxa in a pasture woodland landscape of  
1324 the Jura Moutains (Switzerland). *Veget. Hist. Archeobot.*, 17, 479-495. [https://doi.org/10.1007/s00334-](https://doi.org/10.1007/s00334-008-0143-0)  
1325 [008-0143-0](https://doi.org/10.1007/s00334-008-0143-0)  
1326  
1327 Mazier, F., Broström, A., Bragée, P., Fredh, D., Stenberg, L., Thiere, G., Sugita, S., Hammarlund, D.,  
1328 2015. Two hundred years of land-use change in the South Swedish Uplands: comparison of historical  
1329 map-based estimates with a pollen-based reconstruction using the landscape reconstruction algorithm.  
1330 *Veg. Hist. Archaeobotany*, 24, 555-570. <https://doi.org/10.1007/s00334-015-0516-0>  
1331  
1332 McCave, I.N., 1972. Transport and escape of fine-grained sediment from shelf areas. *Shelf Sediment*  
1333 *Transport*, 225-248.  
1334  
1335 Menier, D., 2004. Morphologie et remplissage des vallées fossiles sud-armoricaines : Apport de la  
1336 stratigraphie sismique. *Mineralogy*, Université Rennes 1, 202 p. [https://tel.archives-ouvertes.fr/tel-](https://tel.archives-ouvertes.fr/tel-00007291)  
1337 [00007291](https://tel.archives-ouvertes.fr/tel-00007291)  
1338

1339 Menier, D., Tessier, B., Proust, J.N., Baltzer, A., Sorrel, P., Traini, C., 2010. The Holocene transgression  
1340 as recorded by incised valley infilling in a rocky coast context with low sediment supply (southern  
1341 Brittany, western France). Bull. Géol. France 181, 2, 115–128.  
1342 <https://doi.org/10.2113/gssgfbull.181.2.115>  
1343  
1344 Menier, D., Augris, C., Briend, C., 2014. Les réseaux fluviaux anciens du plateau continental de  
1345 Bretagne Sud. Editions Quae, 104 p.  
1346  
1347 Mertens, K.N., Verhoeven, K., Verleye, T., Louwye, S., Amorim, A., Ribeiro, S., et al., 2009.  
1348 Determining the absolute abundance of dinoflagellate cysts in recent marine sediments: the *Lycopodium*  
1349 marker-grain method put to the test. Rev. Palaeobot. Palynol. 157, 238–252.  
1350 <https://doi.org/10.1016/j.revpalbo.2009.05.004>  
1351  
1352 Milne, G. A., Long, A.L., Basset, S.E., 2005. Modelling Holocene relative sea-level observations from  
1353 the Caribbean and South Ameri. Quat. Sci Rev., 24, 1183–1202.  
1354 <https://doi.org/10.1016/j.quascirev.2004.10.005>  
1355  
1356 Moffa-Sánchez, P., Hall, I.R., 2017. North Atlantic variability and its links to European climate over the  
1357 last 3000 years. Nat Commun 8, 1726. <https://doi.org/10.1038/s41467-017-01884-8>  
1358  
1359 Mojtahid, M., Durand, M., Coste, P-O., Toucanne, S., Howa, H., Nizou, J., Eynaud, F., Penaud, A.,  
1360 2019. Millennial-scale Holocene hydrological changes in the northeast Atlantic: New insights from ‘La  
1361 Grande Vasière’ mid-shelf mud belt. Holocene 29, 467–480.  
1362 <https://doi.org/10.1177/0959683618816478>  
1363  
1364 Morley, A., Rosenthal, Y., Demenocal, P., 2014. Ocean-atmosphere climate shift during the mid-to-late  
1365 Holocene transition. Earth Planet. Sci. Lett. 388, 18–26. <https://doi.org/10.1016/j.epsl.2013.11.039>  
1366  
1367 Morzadec-Kerfourn, M.-T., 1974. Variations de la ligne de rivage armoricaine au Quaternaire : analyses  
1368 polliniques de dépôts organiques littoraux, Thèse, Université de Rennes 1, 208 p.  
1369  
1370 Morzadec-Kerfourn, M.-T., 1976. La signification écologique des dinoflagellés et leur intérêt pour  
1371 l’étude des variations du niveau marin. Revue de Micropaléontologie 18, 229–235.  
1372  
1373 Morzadec-Kerfourn, M.-T., 1977. Les kystes de Dinoflagellés dans les sédiments récents le long des  
1374 côtes bretonnes. Rev. de Micropaléontologie 20, 157–166.  
1375

1376 Morzadec-Kerfourn, M.-T., 1992. Upper Pleistocene and Holocene dinoflagellate cyst assemblages in  
1377 marine environments of the Mediterranean Sea and the north-west Atlantic coast of France. In: Head,  
1378 M.J., and Wrenn, J.H. (eds.), *Neogene and Quaternary Dinoflagellate Cysts and Acritarchs*: American  
1379 Association of Stratigraphic Palynologists Foundation, Dallas, 121–132.

1380

1381 Morzadec-Kerfourn, M.-T., 1997. Dinoflagellate cysts and the paleoenvironment of Late-Pliocene  
1382 early-pleistocene deposits of Brittany, Northwest France. *Quat. Sci. Rev.* 16, 883–898.

1383

1384 Naughton, F., Bourillet, J.-F., Sanchez Goni, M.F., Turon, J.-L., Jouanneau, J.-M., 2007. Long-term and  
1385 millennial-scale climate variability in northwestern France during the last 8850 years. *Holocene* 17,  
1386 939–953. <https://doi.org/10.1177/0959683607082410>

1387

1388 Olsen, J., Anderson, N.J., Knudsen, M.F., 2012. Variability of the Atlantic Oscillation over the past  
1389 5,200 years. *Nat. Geosci.* 5, 808–812. <https://doi.org/10.1038/ngeo1589>

1390

1391 Olsen, J.L., Mehlenbacher, S.A., Azarenko, A.N., 2000. Hazelnut Pollination. *Hort. Technol.*, 10, 113–  
1392 115. <https://doi.org/10.21273/HORTTECH.10.1.113>

1393

1394 Paillet, Y., Marchand, G., Blanchet, S., Guyodo, J.N., Hamon, G., 2008. Le Villeneuve-Saint-Germain  
1395 dans la néolithisation de la péninsule armoricaine : les débuts d'une enquête, in L. Burnez-Lanotte, M.  
1396 Ilett et P. Allard dir., *Fin des traditions danubiennes dans le Néolithique du Bassin parisien et de la*  
1397 *Belgique (5100-4700 BC), autour des recherches de Claude Constantin*, Mémoire XLIV de la Société  
1398 Préhistorique Française, Co-édition SPF et Presses Universitaire de Namur, 91–111.

1399

1400 Paillet, Y., Nicolas, C. dir., 2019. *Une maison sous les dunes : Beg ar Loued, île Molène, Finistère.*  
1401 *Identité et adaptation des groupes humains en mer d'Iroise à la transition des IIIe – IIe millénaires avant*  
1402 *notre ère*, Ed. Sidestone press, Leiden, 734 p.

1403

1404 Penaud, A., Ganne, A., Eynaud, F., Lambert, C., Coste, P.O., Herlédan, M., Vidal, M., Goslin, J.,  
1405 Stéphan, P., Charia, G., Paillet, Y., Durant, M., Zumaque, J., Mojtahid, M., 2020. Oceanic versus  
1406 continental influences over the last 7 kyrs from a mid-shelf record in the northern Bay of Biscay (NE  
1407 Atlantic). *Quat.Sci. Rev.* 229, 106135. <https://doi.org/10.1016/j.quascirev.2019.106135>

1408

1409 Perez-Belmonte, L., 2008. *Caractérisation environnementale, morphosédimentaire et stratigraphique du*  
1410 *Golfe du Morbihan pendant l'Holocène terminal : Implications Évolutives*. Thèses, Université de  
1411 Bretagne Sud. <https://hal.archives-ouvertes.fr/tel-02382565>

1412



1413 Pingree, RD, Le Cann, B, 1989. Celtic and Armorican slope and shelf residual currents. Prog. Oceanogr.  
1414 23, 303–338. [https://doi.org/10.1016/0079-6611\(89\)90003-7](https://doi.org/10.1016/0079-6611(89)90003-7)  
1415

1416 Proust, J.-N., Menier, D., Guillocheau, F., Guennoc, P., Bonnet, S., Le Corre, C., Rouby, D., 2001. Les  
1417 vallées fossiles de la Vilaine : nature et évolution du prisme sédimentaire côtier du Pléistocène  
1418 armoricain. – Bull. Soc. géol. Fr., 172, 6, 737-749. <https://doi.org/10.2113/172.6.737>  
1419

1420 Puc, M., Kasprzyk, I., 2013. The patterns of *Corylus* and *Alnus* pollen seasons and pollination periods  
1421 in two Polish cities located in different climatic regions. Aerobiologia 29, 495–511.  
1422 <https://doi.org/10.1007/s10453-013-9299-x>  
1423

1424 Reid, P.C., 1975. A regional sub-division of dinoflagellate cysts around the British Isles. The New  
1425 Phytol. 75, 589–603. <https://doi.org/10.1111/j.1469-8137.1975.tb01425.x>  
1426

1427 Reille, M., 1995. Pollen et spores d'Europe et d'Afrique du Nord: supplement 1. Laboratoire de  
1428 Botanique Historique et Palynologie, Marseille, 327 p.  
1429

1430 Reimer, P., Austin, W., Bard, E., Bayliss, A., et al., 2020. The IntCal20 Northern Hemisphere  
1431 Radiocarbon Age Calibration Curve (0–55 cal kBP). Radiocarbon, 62(4), 725–757.  
1432 <https://doi.org/10.1017/RDC.2020.41>  
1433

1434 Rochon, A., Vernal, A.d., Turon, J.-L., Matthießen, J., Head, M., 1999. Distribution of recent  
1435 dinoflagellate cysts in surface sediments from the North Atlantic Ocean and adjacent seas in relation to  
1436 sea-surface parameters. American Association of Stratigraphic Palynologists Contribution Series. 35,  
1437 1–146.  
1438

1439 Rodríguez-Rajo, F. J., Méndez, J., Jato, V., 2005. Environmental factors affecting pollination ecology  
1440 of *Quercus* anemophilous species in North-West Spain. Bot. J. Linn. Soc., 15.  
1441 <https://doi.org/10.1111/j.1095-8339.2005.00460.x>  
1442

1443 Shom, 2012. PROTEUS\_DUNES cruise, RV Pourquoi pas ?, <https://doi.org/10.17600/12030130>  
1444

1445 Sjögren, P., van der Knaap, W.O., van Leeuwen, J.F., 2015. Pollen dispersal properties of Poaceae and  
1446 Cyperaceae: First estimates of their absolute pollen productivities. Rev. Palaeobot. Palynol. 216, 123–  
1447 131. <https://doi.org/10.1016/j.revpalbo.2015.02.004>  
1448

1449 Stéphan, P., Goslin, J., Pailler, Y., Manceau, R., Suanez, S., Van Vliet-Lanoë, B., Hénaff, A., Delacourt,  
1450 C., 2015. Holocene salt-marsh sedimentary infillings and relative sea-level changes in West Brittany  
1451 (France) from foraminifera-based transfer functions. *Boreas* 44, 153–177.  
1452 <https://doi.org/10.1111/bor.12092>  
1453  
1454 Stéphan, P., Verdin, F., Arnaud-Fassetta, G., Bertrand, F., Eynaud, F., García-Artola, A., Bosq, M.,  
1455 Culioli, C., Suanez, S., Coutelier, C., Bertran, P., Colin, A., Costa, S., 2019. Holocene coastal changes  
1456 along the Gironde estuary (SW France): new insights from the North Medoc peninsula beach/dune  
1457 system. *Quaternaire* 30, 47–75. <https://doi.org/10.4000/quaternaire.11172>  
1458  
1459 Stuiver, M., Reimer, P.J., 1993. Extended 14C database and revised CALIB radiocarbon calibration  
1460 program. *Radiocarbon* 35, 215–230.  
1461  
1462 Tisnérat-Laborde, N., Paterne, M., Métivier, B., Arnold, M., Yiou, P., Blamart, D., Raynaud, S., 2010.  
1463 Variability of the northeast Atlantic sea surface D14C and marine reservoir age and the North Atlantic  
1464 Oscillation (NAO). *Quat. Sci. Rev.* 29, 2633–2646. <https://doi.org/10.1016/j.quascirev.2010.06.013>  
1465  
1466 Thornalley, D.J.R., Elderfield, H., McCave, I.N., 2009. Holocene oscillations in temperature and salinity  
1467 of the surface subpolar North Atlantic. *Nature* 457, 711–714. <https://doi.org/10.1038/nature07717>  
1468  
1469 Tréguer, P., Goberville, E., Barrier, N., L’Helguen, S., Morin, P., Bozec, Y., Rimmelin-Maury, P.,  
1470 Czamanski, M., Grossteffan, E., Cariou, T., Répécaud, M., Quéméner, L., 2014. Large and local-scale  
1471 influences on physical and chemical characteristics of coastal waters of Western Europe during winter.  
1472 *J. Mar. Syst.* 139, 79–90. <https://doi.org/10.1016/j.jmarsys.2014.05.019>  
1473  
1474 Turon, J. L., 1984. Le palynoplancton dans l’environnement actuel de l’Atlantique Nord-oriental.  
1475 Evolution climatique et hydrologique depuis le dernier maximum glaciaire. *Mémoires de l’Institut de*  
1476 *Géologie du Bassin d’Aquitaine* 17, 313 pp.  
1477  
1478 van Beek, R., Marguerie, D., Bruel, F., 2018. Land use, settlement, and plant diversity in Iron Age  
1479 Northwest France. *Holocene*, 28(4), 513–528. <https://doi.org/10.1177/0959683617735590>  
1480  
1481 Vanney, J.R., 1977. *Géomorphologie de la marge continentale sud-armoricain*. S.E.D.E.S, Paris, 473 p.  
1482  
1483 Van Nieuwenhove, N., Head, M. J., Limoges, A., Pospelova, V., Mertens, K. N., Matthiessen, J., De  
1484 Schepper, S., de Vernal, A., Eynaud, F., Londeix, L., Marret, F., Penaud, A., Radi, T., Rochon, A., 2020.  
1485 An Overview and Brief Description of Common Marine Organic-Walled Dinoflagellate Cyst Taxa

1486 Occurring in Surface Sediments of the Northern Hemisphere. *Mar. Micropaleontol.* 159, 101814.  
1487 <https://doi.org/10.1016/j.marmicro.2019.101814>  
1488

1489 Visset, L., Sellier, D., L'Helgouach, J., 1995. Le paléoenvironnement de la région de Carnac. Sondage  
1490 dans le marais de Ker dual, La Trinité-sur-Mer (Morbihan). IN : *Revue archéologique de l'ouest*, tome  
1491 12, 57–71. <https://doi.org/10.3406/rao.1995.1025>  
1492

1493 Visset, L., L'Helgouach, J., Bernard, J., 1996. La tourbière submergée de la pointe de Kerpenhir à  
1494 Locmariaquer (Morbihan). Etude environnementale et mise en évidence de déforestations et de pratiques  
1495 agricoles néolithiques. *Revue archéologique de l'ouest* 13, 79–87. <https://doi.org/10.3406/rao.1996.1041>  
1496

1497 Visset, L., Bernard, J., 2006. Evolution du littoral et du paysage, de la presqu'île de Rhuys à la rivière  
1498 d'Étel (Massif armoricain – France), du Néolithique au Moyen Age. *ArcheoSciences* 30, 143–156.  
1499 <https://doi.org/10.4000/archeosciences.315>  
1500

1501 Wall, D., Dale, B., 1966. Living fossils in western Atlantic plankton. *Nature* 211 (5053), 1025–1026.  
1502 <https://doi.org/10.1038/2111025a0>  
1503

1504 Walker, KR., Bambach, R.K., 1971. The significance of fossil assemblages from fine-grained  
1505 sediments: time-averaged communities. Abstracts with programs, Geol. Soc. Am. Annual Meeting,  
1506 Washington. 783–784.  
1507

1508 Walker, M., Gibbard, P., Head, M.J., Berkelhammer, M., Björck, S., Cheng, H., Cwynar, L.C., Fisher,  
1509 D., Gkinis, V., Long, A., Lowe, J., Newnham, R., Rasmussen, S.O., Weiss, H., 2019. Formal  
1510 Subdivision of the Holocene Series/Epoch: A Summary. *J. Geo. Soc. India*, 93, 135–141.  
1511 <https://doi.org/10.1007/s12594-019-1141-9>  
1512

1513 Weber, N., Chaumillon, E., Tesson, M., Garlan, T., 2004. Architecture and morphology of the outer  
1514 segment of a mixed tide and wave-dominated incised valley, revealed by HR seismic reflection  
1515 profiling: The paleo-Charente River, France. *Mar. Geol.*, 207, 17-38.  
1516 <https://doi.org/10.1016/j.margeo.2004.04.001>  
1517

1518 Yonge, C., 1946. On the Habits of *Turritella Communis* Risso. *Journal of the Marine Biological*  
1519 *Association of the United Kingdom*, 26(3), 377–380. <https://doi.org/10.1017/S0025315400012194>  
1520

1521 Zonneveld, K.A., Marret, F., Versteegh, G.J., Bogus, K., Bonnet, S., Bouimetarhan, I., Crouch, E., de  
1522 Vernal, A., Elshanawany, A., Edwards, L., Esper, O., Forke, S., Grøsfjeld, K., Henry, M., Holzwarth,

1523 U., Kieft, J.F., Kim, S.Y., Ladouceur, S., Ledu, D., Chen, L., Limoges, A., Londeix, L., Lu, S.H.,  
1524 Mahmoud, M.S., Marino, G., Matsuoka, K., Matthiessen, J., Mildenhall, D.C., Mudie, P., Neil, H.L.,  
1525 Pospelova, V., Qi, Y., Radi, T., Richerol, T., Rochon, A., Sangiorgi, F., Solignac, S., Turon, J.L.,  
1526 Verleye, T., Wang, Y., Wang, Z., Young, M., 2013. Atlas of modern dinoflagellate cyst distribution  
1527 based on 2405 data points. *Rev. Palaeobot. Palynol.* 191, 1–197.  
1528 <https://doi.org/10.1016/j.revpalbo.2012.08.003>  
1529  
1530 Zumaque, J., Eynaud, F., de Vernal, A., 2017. Holocene paleoceanography of the Bay of Biscay:  
1531 evidence for west-east linkages in the North Atlantic based on dinocyst data. *Palaeogeogr.*  
1532 *Palaeoclimatol. Palaeoecol.* 468, 403–413. <https://doi.org/10.1016/j.palaeo.2016.12.031>